NBS SPECIAL PUBLICATION 400-47

U.S. DEPARTMENT OF COMMERCE / National Bureau of Standards

Semiconductor Measurement Technology:

The Theoretical and Experimental Study of the Temperature and Dopant Density Dependence of Hole Mobility, Effective Mass, and Resistivity in Boron-Doped Silicon

NATIONAL BUREAU OF STANDARDS

The National Bureau of Standards[1] was established by an act of Congress on March 3, 1901. The Bureau's overall goal is to strengthen and advance the Nation's science and technology and facilitate their effective application for public benefit. To this end, the Bureau conducts research and provides: (1) a basis for the Nation's physical measurement system, (2) scientific and technological services for industry and government, (3) a technical basis for equity in trade, and (4) technical services to promote public safety. The Bureau's technical work is performed by the National Measurement Laboratory, the National Engineering Laboratory, and the Institute for Computer Sciences and Technology.

THE NATIONAL MEASUREMENT LABORATORY provides the national system of physical and chemical and materials measurement; coordinates the system with measurement systems of other nations and furnishes essential services leading to accurate and uniform physical and chemical measurement throughout the Nation's scientific community, industry, and commerce; conducts materials research leading to improved methods of measurement, standards, and data on the properties of materials needed by industry, commerce, educational institutions, and Government; provides advisory and research services to other Government agencies; develops, produces, and distributes Standard Reference Materials; and provides calibration services. The Laboratory consists of the following centers:

Absolute Physical Quantities[2] — Radiation Research — Thermodynamics and Molecular Science — Analytical Chemistry — Materials Science.

THE NATIONAL ENGINEERING LABORATORY provides technology and technical services to the public and private sectors to address national needs and to solve national problems; conducts research in engineering and applied science in support of these efforts; builds and maintains competence in the necessary disciplines required to carry out this research and technical service; develops engineering data and measurement capabilities; provides engineering measurement traceability services; develops test methods and proposes engineering standards and code changes; develops and proposes new engineering practices; and develops and improves mechanisms to transfer results of its research to the ultimate user. The Laboratory consists of the following centers:

Applied Mathematics — Electronics and Electrical Engineering[2] — Mechanical Engineering and Process Technology[2] — Building Technology — Fire Research — Consumer Product Technology — Field Methods.

THE INSTITUTE FOR COMPUTER SCIENCES AND TECHNOLOGY conducts research and provides scientific and technical services to aid Federal agencies in the selection, acquisition, application, and use of computer technology to improve effectiveness and economy in Government operations in accordance with Public Law 89-306 (40 U.S.C. 759), relevant Executive Orders, and other directives; carries out this mission by managing the Federal Information Processing Standards Program, developing Federal ADP standards guidelines, and managing Federal participation in ADP voluntary standardization activities; provides scientific and technological advisory services and assistance to Federal agencies; and provides the technical foundation for computer-related policies of the Federal Government. The Institute consists of the following centers:

Programming Science and Technology — Computer Systems Engineering.

[1]Headquarters and Laboratories at Gaithersburg, MD, unless otherwise noted; mailing address Washington, DC 20234.
[2]Some divisions within the center are located at Boulder, CO 80303.

Semiconductor Measurement Technology:

The Theoretical and Experimental Study of the Temperature and Dopant Density Dependence of Hole Mobility, Effective Mass, and Resistivity in Boron-Doped Silicon

Sheng S. Li

Department of Electrical Engineering
University of Florida
Gainesville, Florida 32611

This activity was supported by

The Defense Advanced Research Projects Agency
and
The National Science Foundation

U.S. DEPARTMENT OF COMMERCE

Luther H. Hodges, Jr., Under Secretary

Jordan J. Baruch, Assistant Secretary for Science and Technology

NATIONAL BUREAU OF STANDARDS, Ernest Ambler, Director

Issued November 1979

Library of Congress Cataloging in Publication Data

Li, Sheng S 1938-

The theoretical and experimental study of the temperature and dopant density dependence of hole mobility, effective mass, and resistivity in boron-doped silicon.

(Semiconductor measurement technology) (NBS special publication ; 400-47)

"This activity was supported by the Defense Advanced Research Projects Agency and the National Science Foundation."

Bibliography: p.

Includes index.

Supt. of Docs. no.: C13.10:400-47

1. Holes (electron deficiencies). 2. Semiconductor doping. 3. Silicon--defects. I. United States. Defense Advanced Research Projects Agency. II. United States. National Science Foundation. III. Title. IV. Series. V. Series: United States. National Bureau of Standards. Special publication ; 400-47.

QC100.U57 no. 400-47 [QC611.6.H6] 602'.1s [537.6'22] 78-24185

National Bureau of Standards Special Publication 400-47

Nat. Bur. Stand. (U.S.), Spec. Publ. 400-47, 50 pages (Nov. 1979)

CODEN: XNBSAV

U.S. GOVERNMENT PRINTING OFFICE

WASHINGTON: 1979

For sale by the Superintendent of Documents, U.S. Government Printing Office, Washington, D.C. 20402

Stock No. 003-003-02140-7 Price $2.25

(Add 25 percent additional for other than U.S. mailing).

☆ U.S. GOVERNMENT PRINTING OFFICE: 1979 O—311-046 (310)

TABLE OF CONTENTS

LIST OF FIGURES

LIST OF SYMBOLS*

E Energy of holes (eV)

E_A Acceptor energy level (eV)

E_F Fermi energy level (eV)

E_G Energy band gap (eV)

E_N Binding energy of neutral acceptors (eV)

E_V Valence band edge (eV)

h Planck's constant (= 6.625×10^{-34}), $\hbar = h/2\pi$

k_o Boltzmann's constant (= 1.38×10^{-23})

m_o Free electron mass (= 9.1×10^{-31})

m^*_{C1} Conductivity effective mass in heavy hole band (in units of m_o)

m^*_{C2} Conductivity effective mass in light-hole band (in units of m_o)

m^*_{C3} Conductivity effective mass in spin-orbit-split (SO) band (in units of m_o)

m^*_{D1} Density-of-states effective mass in heavy-hole band (in units of m_o)

m^*_{D2} Density-of-states effective mass in light-hole band (in units of m_o)

m^*_{D3} Density-of-states effective mass in SO band (in units of m_o)

m^*_D Total density-of-states effective mass of hole (in units of m_o)

N_A Total boron density (cm^{-3})

N^-_A Ionized boron density (cm^{-3})

N_N Neutral boron density (cm^{-3})

N_V Effective density of valence band states (cm^{-3})

---

*Unless stated otherwise, all units are in MKS.

p	Hole density (cm^{-3})
p'	Effective screening hole density (cm^{-3})
q	Electronic charge ($= 1.6 \times 10^{-19}$)
T	Absolute temperature
ε	Reduced energy of carrier ($= E/k_o T$)
ε_o	Free space permittivity ($= 8.854 \times 10^{-12}$)
ε_s	Permittivity of silicon ($= 4\pi \times 11.7 \times \varepsilon_o$)
μ_L	Lattice scattering mobility ($cm^2/V \cdot s$)
μ_I	Ionized impurity scattering mobility ($cm^2/V \cdot s$)
μ_N	Neutral impurity scattering mobility ($cm^2/V \cdot s$)
μ_{LI}	Combined lattice and ionized impurity scattering mobility ($cm^2/V \cdot s$)
μ_p	Total hole conductivity mobility ($cm^2/V \cdot s$)
ρ	Resistivity ($\Omega \cdot cm$)
τ	Relaxation time

PREFACE

This study was carried out at the University of Florida as a part of the Semiconductor Technology Program in the Electron Devices Division at the National Bureau of Standards. The Semiconductor Technology Program serves to focus NBS research to enhance the performance, interchangeability, and reliability of discrete semiconductor devices and integrated circuits through improvements in measurement technology for use in specifying materials and devices in national and international commerce and for use by industry in controlling device fabrication processes. This work was supported by the Defense Advanced Research Projects Agency, ARPA Order 2397, Program Code 7Y10, through the National Bureau of Standards Semiconductor Technology Program.

ACKNOWLEDGMENTS

The author would like to express his special thanks to Dr. W. M. Bullis for his critical review of the manuscript and for his valuable comments. He would also like to acknowledge stimulating discussions and assistance on the part of Dr. M. G. Buehler and W. R. Thurber during the course of this study. The planar four-probe test structures used in the present resistivity measurements were fabricated by Y. M. Liu of NBS. R. L. Mattis and W. R. Thurber provided the information of dopant density in these test samples. Thanks are also due L. C. Linares for effective mass calculations and for checking other theoretical calculations described in this work. The author gratefully acknowledges the critical review and comments of Dr. A. H. Kahn of NBS. Typing and proofreading of the final draft was done by Jo Halapatz, Jane Walters, and Elaine Cohen.

Semiconductor Measurement Technology:
THE THEORETICAL AND EXPERIMENTAL STUDY OF THE TEMPERATURE AND DOPANT DENSITY DEPENDENCE OF HOLE MOBILITY, EFFECTIVE MASS, AND RESISTIVITY IN BORON-DOPED SILICON

By

SHENG S. LI
Department of Electrical Engineering
University of Florida
Gainesville, FL 32611

ABSTRACT

Theoretical expressions for computing resistivity and conductivity mobility of holes as functions of dopant density and temperature have been derived for boron-doped silicon. The model is applicable for dopant densities from 10^{13} to 3×10^{18} cm^{-3} and temperatures between 100 and 400 K.

Using a three-band [i.e., heavy-hole, light-hole, and spin-orbit split (SO) bands] model, the hole mobility was calculated by properly combining the contributions from scattering by lattice phonons, ionized impurities, and neutral impurities. In addition, the effects of hole-hole (h-h) scattering and nonparabolicity of the light-hole band were taken into account in the mobility formulation.

To verify our theoretical calculations, resistivity measurements on nine boron-doped silicon slices with dopant densities from 4.5×10^{14} to 3.2×10^{18} cm^{-3} were performed for $100 \leq T \leq 400$ K, using a planar four-probe square-array test structure. Agreement between our calculated and measured resistivity values was within 6 percent over the entire range of dopant density and temperature studied here. Excellent agreement (within ±5 percent) between our calculated hole mobility values and those of Thurber *et al.* was obtained for $N_A \leq 10^{18}$ cm^{-3} for boron-doped silicon, while discrepancies between our calculated values and those of Wagner were found for boron densities greater than 10^{17} cm^{-3}. These discrepancies are attributed to Wagner's neglect of the effect of deionization of boron impurities at higher dopant densities (i.e., he assumed hole density equal to the total boron density).

Finally, formulations for the density-of-states effective mass, conductivity effective mass, and Hall effective mass are described, and the results are applied to the calculations of hole masses in boron-doped silicon for $10^{14} \leq N_A \leq 10^{18}$ cm^{-3} and $50 \leq T \leq 500$ K.

Key Words: Boron-doped silicon; dopant density; effective mass; hole mobility; ionized impurity scattering mobility; lattice scattering mobility; neutral impurity scattering mobility; *p*-type silicon; resistivity; scattering mechanisms.

1. INTRODUCTION

Although a considerable amount of work on mobility and resistivity has been published [1-11], because of the complexity of the valence band structure and of the various scattering mechanisms involved, only limited amount of work has been reported on mobility calculations in *p*-type silicon. For example, Ottaviani *et al.* [1] have developed a microscopic theoretical model applicable only to computation of ohmic mobility in high purity *p*-type silicon in which nonpolar optical and acoustical phonon scattering is dominant. In their theoretical analysis, they have shown the necessity of considering band nonparabolicity in the mobility formulation, and have pointed out that the band warping effect is secondary in

importance to that of nonparabolicity. The lattice mobilities for holes in p-type silicon are well established for temperatures between 50 and 400 K [1-6]. Braggins [4] has analyzed carrier concentration and hole mobility in boron-doped silicon from Hall effect and resistivity measurements. His calculations, which are based on a three-band model and the relaxation time approximation, yield impurity densities which appear to agree well with Hall effect data for boron densities less than 5×10^{16} cm^{-3}. Large discrepancies exist among the published hole mobility data [7-10] for dopant densities greater than 10^{16} cm^{-3}; no adequate theoretical model is available for mobility and resistivity calculations in p-type silicon that is valid over the full range of dopant densities and temperatures studied here.

The purpose of this paper is to present theoretical and experimental investigations of the dopant density and temperature dependence of hole mobility and resistivity in boron-doped silicon for $10^{13} \leq N_A \leq 3 \times 10^{18}$ cm^{-3} and $100 \leq T \leq 400$ K.

To overcome difficulties in effective mass calculations and mobility formulation, the valence band structure of silicon was approximated by a three-band model consisting of a spherical, parabolic heavy-hole band; a spherical, nonparabolic light-hole band; and a spherical, parabolic split-off band [12]. Together with this model, the relaxation time approximation was used to develop theoretical expressions for mobility of holes in p-type silicon. Scattering mechanisms due to lattice (i.e., acoustical and optical phonons), ionized impurity, and neutral impurity scattering are considered over the entire range of dopant densities and temperatures studied. In addition, the effects of hole-hole (h-h) scattering on the lattice and ionized impurity scattering mobilities are also taken into account. In view of the complex nature of heavy doping effects and the uncertainties in accounting for hole density and impurity density at high dopant densities, the present analysis has been restricted to boron densities up to 3×10^{18} cm^{-3}, a dopant density range in which the use of Boltzmann statistics is valid.

In section 2 the theoretical approach is described, presenting the results of effective mass calculations and mobility and resistivity formulations. The appropriate scattering mechanisms for holes are discussed. In section 3 the theoretical and experimental results are compared and discussed. Section 4 summarizes the main conclusions derived from this work. The Appendix is a paper by L. C. Linares and S. S. Li on the temperature dependence of effective masses in p-type silicon.

2. THEORETICAL APPROACH

Presented in this section are the results of calculations of hole effective mass and the mobility and resistivity formulations for p-type silicon. Theoretical expressions for hole mobility are derived by considering contributions from lattice, ionized impurity, and neutral impurity scattering. The effects of h-h scattering and light-hole band nonparabolicity are also taken into account in the mobility formulation.

A. Valence Band and Hole Effective Masses

The heavy-hole and light-hole bands of silicon have an extremum at $k = 0$ and are degenerate there. The constant energy surfaces for this case are warped spheres. The derivation

of an expression for a valence band effective mass which incorporates the nonparabolic nature of the individual bands begins with a simplified model of the warped structure based on the work of Kane [13] and Barber [12]. In this model, the heavy-hole band is characterized by holes with an energy-independent but direction-dependent effective mass, and the light-hole band is characterized by holes with an effective mass which is both energy- and direction-dependent. The split-off (SO) band is separated from the heavy- and light-hole bands at k = 0 by an energy $\Delta = 0.044$ eV, and is characterized by an isotropic, energy-dependent effective mass. Thus, the heavy-hole band is treated as parabolic for the range of temperatures considered in this work, while the light-hole band is parabolic only for very low values of k. At higher values of k, the light-hole band has an energy-dependent curvature which takes on the same characteristics as the heavy-hole band for energies greater than 0.02 eV.

Based on the above band model, effective masses and density-of-states effective masses have been calculated for holes in each of the three valence bands. Details of the calculations are provided in the Appendix; the results are summarized in table 1.

Table 1. Density-of-States and Conductivity Effective Masses of Holes in p-Type Silicon for $N_A = 10^{15}$ cm^{-3} and $100 \leq T \leq 400$ K.

T(K)	100	150	200	250	300	350	400
m^*_{D1}	0.5503	0.5547	0.5592	0.5638	0.5685	0.5733	0.5782
m^*_{D2}	0.2481	0.3087	0.3527	0.3865	0.4118	0.4332	0.4496
m^*_{D3}	0.238	0.240	0.242	0.244	0.246	0.248	0.250
m^*_{D}	0.6570	0.7023	0.7340	0.7624	0.7865	0.8081	0.8265
m^*_{C1}	0.4271	0.4322	0.4375	0.4429	0.4484	0.4541	0.4599
m^*_{C2}	0.3284	0.4337	0.4886	0.5172	0.5324	0.5383	0.5380
m^*_{C3}	0.2399	0.2427	0.2475	0.2512	0.2532	0.2549	0.2597
m^*_{C}	0.3592	0.4181	0.4497	0.4673	0.4785	0.4865	0.4904

Note: Definitions of density-of-states and conductivity effective masses of holes in each band are given in the Appendix.

B. Mobility Formulations and Scattering Mechanisms

The calculation of hole mobility in p-type silicon can be carried out by first computing the hole mobilities in the heavy-hole, the light-hole, and the SO band separately; the overall mobility of holes is then calculated as a weighted average of these one-band mobilities over the individual hole densities in each valence band. The scattering mechanisms considered in this work include (a) intraband optical and acoustical phonon scattering, (b) intraband ionized and neutral impurity scattering, (c) interband acoustical phonon scattering, and (d) the h-h scattering. In addition, the effect of nonparabolicity of the light-hole band is also taken into account in the mobility calculations. Following is a

discussion of the various scattering mechanisms cited above and a presentation of the appropriate mobility formulation for each scattering process in p-type silicon.

i. Lattice Scattering Mobility

The published hole conductivity mobility data for lightly doped p-type silicon exhibit a $T^{-2.5\pm0.2}$ temperature dependence for $150 < T < 400$ K [1-6]. Since acoustical phonon scattering only leads to theoretical mobility following a $T^{-1.5}$ law, additional scattering due to nonpolar optical phonons, interband acoustical phonons, and the effects of hole-hole scattering and nonparabolicity of the valence band should be included to explain this discrepancy [2]. The nonparabolic band structure in the light-hole band and the temperature dependence of the energy band gap lead to a dependence of hole effective masses on temperature in each band; this is shown in table 1.

The relaxation times for scattering by acoustical phonons include both the possibility of interband as well as intraband transitions; interband scattering has been considered only between the light- and heavy-hole bands. The treatment of the acoustical phonons has been based on the theory of Bir, Normantas, and Pikus [14] where the relaxation times can be expressed in terms of a single constant, τ_o, which controls the overall magnitude of the scattering. Both transverse and longitudinal phonons participate in the scattering. Braggins [4] has applied their theory to evaluate the lattice mobility for p-type silicon. His results for the acoustical phonon relaxation times may be written as

$$\frac{1}{\tau_{ac1}} = \frac{0.959}{\tau_o} m_{D1}^{*3/2} T^{3/2} \varepsilon^{1/2} \tag{1}$$

$$\frac{1}{\tau_{ac2}} = \frac{1.61}{\tau_o} m_{D2}^{*3/2} T^{3/2} \varepsilon^{1/2} \tag{2}$$

$$\frac{1}{\tau_{ac12}} = \frac{0.224}{\tau_o} \frac{m_{D1}^{*5/2}}{m_{D2}^{*}} m_{D1}^{*3/2} T^{3/2} \varepsilon^{1/2} \tag{3}$$

$$\frac{1}{\tau_{ac21}} = \frac{0.224}{\tau_o} m_{D2}^{*3/2} T^{3/2} \varepsilon^{1/2}, \tag{4}$$

and

$$\frac{1}{\tau_{ac3}} = \frac{1}{\tau_o} (\varepsilon - \Delta/k_o T)^{1/2} T^{3/2} \tag{5}$$

where

$$\frac{1}{\tau_o} = \frac{2^{1/2} k_o^{3/2} E_1^2}{\pi h^4 \rho_s u_s^2} \tag{6}$$

Equations (1) to (4) represent the acoustical phonon scattering times for the heavy- and light-hole bands taking into account the interband and intraband transitions, while eq (5) is the expression for the intraband acoustical phonon scattering in the split-off band.

The relaxation time for scattering by the nonpolar optical phonons is given by [14]

$$\tau_{oi}^{-1} = \frac{m_{Di}^{3/2}}{\tau_o} W\theta T^{1/2} \left\{ \left(\eta_o + 1\right) \left(\varepsilon - \theta/T\right)^{1/2} + \eta_o \left(\varepsilon + \theta/T\right)^{1/2} \right\}, \tag{7}$$

where θ is the Debye temperature, $\eta_o = [\exp(\theta/T) - 1]^{-1}$ is the phonon distribution function, and W is a constant which determines the relative coupling strength of the holes to the optical phonon mode compared to the acoustical phonon mode. In eq (7) the band index, i = 1, 2, or 3, denotes the heavy-hole, light-hole, or the SO band, respectively. This notation will be used for other scattering processes as well throughout the text. The lattice mobility in each of the three valence bands can be calculated from

$$\mu_{Li} = \frac{q\langle\tau_{Li}\rangle}{m_{ci}^*}, \tag{8}$$

where

$$\langle\tau_{Li}\rangle = \frac{4}{3\sqrt{\pi}} \int_0^\infty \tau_{Li}\, \varepsilon^{3/2}\, e^{-\varepsilon}\, d\varepsilon$$

and

$$\tau_{Li} = \left[\tau_{aci}^{-1} + \tau_{oi}^{-1}\right]^{-1}. \tag{9}$$

Here τ_{aci} can be evaluated from eqs (1) through (6) and τ_{oi} from eq (7).

The total lattice mobility, based on a three-band model, can be expressed by

$$\mu_L = \left[\mu_{L1} + \mu_{L2} \left(\frac{m_{D2}^*}{m_{D1}^*}\right)^{3/2} + \mu_{L3} \left(\frac{m_{D3}^*}{m_{D1}^*}\right)^{3/2} \cdot \exp\left(-\Delta/k_o T\right) \right] \cdot \left[1 + \left(\frac{m_{D2}^*}{m_{D1}^*}\right)^{3/2} + \left(\frac{m_{D3}^*}{m_{D1}^*}\right)^{3/2} \cdot \exp\left(-\Delta/k_o T\right) \right]^{-1}, \tag{10}$$

where μ_{L1}, μ_{L2}, and μ_{L3} are lattice mobilities calculated from eq (8) for the heavy-hole, light-hole, and the SO band, respectively. Values of μ_L calculated from eqs (1) through (10) for boron-doped silicon are listed in table 2 for $100 \leq T \leq 400$ K. Table 3 lists the physical constants used in the present calculations.

Table 2. Hole Lattice Mobility for Boron-Doped Silicon Calculated From eq (8), Using the Parameters Listed in Table 3.

T(K)	100	150	200	250	300	350	400
$\mu_L \left(\frac{cm^2}{V \cdot s}\right)$	6020	2287	1204	706	465	336	261

Table 3. Material Parameters Used in Calculating Lattice Mobility in Boron-Doped Silicon.

Optical phonon temperature, θ, (K) [1]	735.0
Acoustical deformation potential constant, E_1 (eV) [1]	8.718
W: Coupling constant between optical and acoustical phonon mode*	0.4
Material density, ρ_s (g/cm^3) [1]	2.329
Velocity of acoustical wave, v_s (cm/s) [1]	9.04×10^5
τ_o	5.8×10^{-10}

*$W = \frac{D_o^2 h^2 v_s^2}{2k_o^2 E_1^2 \theta^2}$; $D_o = 8.3025 \times 10^8$ eV/cm is the optical deformation potential constant.

ii. Ionized Impurity Scattering Mobility

In pure silicon at room temperature, the main contribution to carrier mobility comes from lattice scattering. However, as dopant density increases or temperature decreases, the role of ionized impurity scattering becomes more important. Theories for ionized impurity scattering have been developed previously by Brooks [15] and Herring [16] and by Conwell and Weisskopf [17]. The Brooks-Herring (B-H) formula has been widely used in mobility calculations for several semiconductors including silicon. The B-H formula can be written as

$$\mu_{ii} = \frac{2^{7/2} \varepsilon_s^2 m_{Di}^{1/2} (k_o T)^{3/2}}{\pi^{3/2} q^3 m_{Ci}^* N_I G(b_i)} \times 10^{-2}, \tag{11}$$

where i = 1, 2, or 3 is the band index and

$$G(b_i) = \ln(b_i+1) - \frac{b_i}{(b_i+1)} , \tag{12}$$

$$b_i = \frac{24\pi m_{Di}^* \varepsilon_s (k_o T)^2}{q^2 h^2 p'} \times 10^{-6} \tag{13}$$

and

$$p' \simeq p + N_A^-(1 - N_A^-/N_A), \text{ for } N_D = 0 \tag{14}$$

The total ionized impurity scattering mobility is calculated from

$$\mu_I = \left[\mu_{I1} + \mu_{I2} \left(\frac{m^*_{D2}}{m^*_{D1}} \right)^{3/2} + \mu_{I3} \left(\frac{m^*_{D3}}{m^*_{D1}} \right)^{3/2} \cdot \exp\left(-\Delta / k_o T \right) \right] \cdot \left[1 + \left(\frac{m^*_{D2}}{m^*_{D1}} \right)^{3/2} + \left(\frac{m^*_{D3}}{m^*_{D1}} \right)^{3/2} \cdot \exp\left(-\Delta / k_o T \right) \right]^{-1}, \tag{15}$$

where μ_{I1}, μ_{I2}, and μ_{I3} are calculated from eq (11) for the heavy-hole, light-hole, and the SO band, respectively.

Note that eq (11) does not include such effects as the variation of dielectric constant around the impurity due to a position-dependent screening which may become important for the heavily doped case. Since analysis is restricted to $N_A \leq 3 \times 10^{18}$ cm^{-3}, neglecting this variation should not introduce an appreciable error in the mobility calculations.

iii. Neutral Impurity Scattering Mobility

Although neutral impurity scattering may not be as important as other scattering mechanisms discussed above in the range of dopant density and temperature considered here, it becomes important at low temperatures or at high dopant densities. For completeness, this scattering mechanism is included in the mobility formulation. The mobility formula derived by Sclar [18] is employed here for neutral impurity scattering. Sclar used his calculation of the scattering from a three-dimensional square well to estimate the influence of a weakly bound state on the scattering. From his derivation one obtains

$$\mu_{Ni} = 0.82\, \mu_{Ei} \left[\frac{2}{3} \left(\frac{k_o T}{E_N} \right)^{1/2} + \frac{1}{3} \left(\frac{E_N}{k_o T} \right)^{1/2} \right], \tag{16}$$

where

$$E_N = 1.135 \times 10^{-19} (m^*_D / m_o)(\varepsilon_o / \varepsilon_s)^2 \tag{17}$$

and

$$\mu_{Ei} = \frac{2\pi^3 q^3 m^*_{Di}}{5 N_N \varepsilon_s h^3} \times 10^{-2} . \tag{18}$$

Equation (18) is the mobility expression derived by Erginsoy [19] for neutral impurity scattering, based on the partial wave expansion approximation.

The total neutral impurity scattering mobility can be computed from

$$\mu_N = \left[\mu_{NI} + \mu_{N2} \left(\frac{m^*_{D2}}{m^*_{D1}} \right)^{3/2} + \mu_{N3} \left(\frac{m^*_{D3}}{m^*_{D1}} \right)^{3/2} \cdot \exp\left(-\Delta / k_o T \right) \right] \cdot \left[1 + \left(\frac{m^*_{D2}}{m^*_{D1}} \right)^{3/2} + \left(\frac{m^*_{D3}}{m^*_{D1}} \right)^{3/2} \cdot \exp\left(-\Delta / k_o T \right) \right]^{-1}, \tag{19}$$

where μ_{N1}, μ_{N2}, and μ_{N3} are calculated from eqs (16) through (18).

iv. Effect of Hole-Hole Scattering

The mobility formulas given in eqs (1) through (19) neglect the effect of h-h scattering. The importance of including electron-electron (e-e) scattering in *n*-type silicon has been discussed in detail previously [20]. In this section the effect of h-h scattering in *p*-type silicon is discussed. The e-e and h-h scattering events, while not directly producing a change in total momentum, provide a mechanism for the redistribution of momentum gained from the electric field. The maximum effect of h-h scattering can be readily calculated (by classical treatment) if the distribution function is Maxwellian and centered about the drift velocity. Assuming $\tau = aE^s$ and by analogy of e-e scattering, it can be shown that the ratio of hole mobilities with and without h-h scattering is given by

$$\gamma_{hh} = \frac{\mu_{hh}}{\mu_o} = \frac{\langle v_{hh} \rangle}{\langle v_o \rangle} = \frac{1}{\langle \tau \rangle \langle \tau^{-1} \rangle} = \Gamma^2(5/2)\left[\Gamma\left(\frac{5}{2} + s\right)\Gamma\left(\frac{5}{2} - s\right)\right]^{-1} \qquad (20)$$

For acoustical phonon scattering with $s = -\frac{1}{2}$, eq (20) predicts a value for $r_{hh} = 9\pi/32 \simeq 0.88$, while for ionized impurity scattering $s = \frac{3}{2}$ and $\gamma_{hh} = 3\pi/32 \simeq 0.29$.

It is noted that γ_{hh} given by eq (20) shows no dependence on hole density and temperature. A more rigorous treatment to account for the effect of carrier-carrier scattering on the ionized impurity scattering mobility has been developed by Luong and Shaw (L&S) [21], using a one-particle-like approximation from the Hartree-Fock theory. Applying their (L&S) theory to the case of the effect of h-h scattering on ionized impurity scattering, the B-H formula [i.e., eq (11)] is reduced by a factor which can be expressed in closed form:

$$\gamma_{hhI} = (N_A^-/p')[1 - \exp(-p'/N_A^-)], \qquad (21)$$

where N_A^- is the ionized acceptor density, and p' is the screening hole density given by eq (14).

In contrast to the classical formula [i.e., eq (20)], eq (21) predicts a dependence of γ_{hhI} on hole density and, hence, temperature. Values of γ_{hhI} may vary between 0.432 and 0.632, depending on the degree of ionization of the shallow acceptor impurities.

A comparison of the values, γ_{hhI}, calculated from eqs (20) and (21) indicates that the classical formula overestimates the h-h scattering effect. Furthermore, by correcting lattice and ionized impurity scattering mobilities separately, the effect of h-h scattering may also be overestimated. To overcome these difficulties, a semi-empirical formula is derived based on eq (20) to correct the effect of h-h scattering on the lattice scattering mobility, and eq (21) has been retained for correcting the effect of h-h scattering on ionized impurity scattering mobility. This will be discussed later.

v. Hole Mobility vs. Dopant Density and Temperature

Following is a discussion of the mobility calculations for *p*-type silicon for dopant densities from 10^{13} to 3×10^{18} cm^{-3} and temperatures between 100 and 400 K. The combined

hole mobility due to both lattice and ionized impurity scattering contributions is calculated according to the mixed scattering formula [22]:

$$\mu_{LI} = \mu_L \left\{ 1 + X^2 [Ci(X)\cos X + \sin X(Si(X) - \frac{\pi}{2})] \right\} , \tag{22}$$

where

$$X^2 = 6\mu_L/\mu_I \quad . \tag{23}$$

Equation (22) is obtained by averaging the reciprocal sum of τ_L^{-1} and τ_L^{-2} over the Maxwellian distribution. Here, Ci(X) and Si(X) are the cosine and sine integrals of X, respectively; μ_L and μ_I are given, respectively, by eqs (10) and (15) when the effect of h-h scattering is neglected.

The effect of h-h scattering can be included by incorporating the mobility reduction factor, γ_{hh}, given in eq (20) for lattice scattering mobility and in eq (21) for ionized impurity scattering mobility, into eq (23) to correct the values of μ_L and μ_I.

Equation (22) allows the calculations of μ_{LI} for $10^{13} \leq N_A \leq 3 \times 10^{18}$ cm^{-3} and $100 \leq T \leq 400$ K. When neutral impurity scattering is included, the total mobility may be computed from the expression

$$\mu_p = [\mu_{LI}^{-1} + \mu_N^{-1}]^{-1} , \tag{24}$$

where μ_{LI} and μ_N are given by eqs (22) and (19), respectively.

The use of eq (24) for mobility calculations may be considered as a good approximation since neutral impurity scattering, being energy-independent, does not affect any contributions from μ_L and μ_I. Calculations of μ_N indicated that the contribution from neutral impurity scattering to total hole mobility is less than 10 percent over the entire range of dopant densities and temperatures studied here. As a result, the error introduced by this approximation is expected to be negligibly small.

The procedure for incorporating the effect of h-h scattering on the lattice scattering mobility for *p*-type silicon is similar to that used for *n*-type silicon [21]. For example, for acoustical phonon scattering, it is assumed that γ_{hh} decreases linearly with increasing dopant density from $\gamma_{hh} = 1$ at $N_A = 10^{15}$ cm^{-3} to a maximum value of $\gamma_{hh} = \frac{9\pi}{32} \simeq 0.88$ for $N_A \geq 3 \times 10^{17}$ cm^{-3}, as predicted by eq (20) [i.e., $\gamma_{hh} = 1.0 - 0.008\ N_A/(2 \times 10^{17})$ is used in the calculation]. This provides the best fit to the experimental data for the range of dopant densities and temperatures studied. This approximation may also offset the possible overestimation of the h-h scattering effect by the classical formula discussed earlier. For ionized impurity scattering, γ_{hhI} is calculated from eq (21) which is applicable for the entire dopant density and temperature range considered here. The mobility reduction factor for optical phonon scattering is evaluated numerically using eq (20). For neutral impurity scattering, no correction is needed since τ_N is independent of energy.

vi. Resistivity *vs.* Dopant Density and Temperature

The resistivity for *p*-type silicon is calculated from

$$\rho = \frac{1}{q\,\mu_p\,p} \,, \tag{25}$$

where μ_p is the hole mobility given by eq (24), and the hole density for the nondegenerate case is

$$p = p_1 + p_2 + p_3 = N_v \exp\left[-\frac{E_F - E_V}{k_o T}\right] , \tag{26}$$

where $N_v = 2\left[\frac{2\pi m^* k_o T}{h^2}\right]^{3/2}$ is the effective density of valence band states, and p_1, p_2, and p_3 are hole densities in the heavy-hole, light-hole, and the SO bands, respectively.

In order to calculate hole mobility and resistivity from eqs (24) and (25), it is necessary to know the exact ionized and neutral impurity densities so that individual scattering contributions and hole density can be evaluated. This is done as follows:

The ionized boron densities for boron-doped silicon are computed by solving the charge balance equation for the Fermi energy by the iteration procedure. Since the minority carrier density is negligible, the charge balance equation for uncompensated p-type silicon is simply*

$$p \simeq N_A^- \,, \tag{27}$$

where [23]

$$N_A^- = \frac{N_A}{1 + [4 + 2\exp(-\frac{\Delta}{k_o T})]\exp[(E_A - E_F)/k_o T]} \tag{28}$$

is the ionized acceptor density, and $\Delta = 0.044$ eV. Equation (28) is used to include the contribution from the heavy- and light-hole bands and the SO band.

Experimental evidence indicates that the acceptor ionization energy E_A is not a constant, but decreases with increasing dopant density [24,25]. A study by Penin *et al.* [25] of heavily doped silicon over the temperature range from 4 to 300 K shows no evidence of an ionization energy for shallow impurities such as phosphorus or boron at impurity densities greater than 3×10^{18} cm^{-3}. The dependence of ionization energy on dopant density for boron-doped silicon can be expressed by [22]

$$E_A \simeq 0.0438 - 3.037 \times 10^{-8}\, N_A^{1/3} \,. \tag{29}$$

With the help of eqs (26) through (29), the hole density and fraction of ionized boron density can be calculated as functions of dopant density and temperature.

---

*A more general form of the charge balance equation is $N_A^- - N_D^+ = p - n$, which should be used if n and N_D^+ are not negligible compared to p and N_A^-, respectively.

3. RESULTS AND DISCUSSIONS

Using the theoretical expressions derived in section 2, the hole mobility and resistivity have been calculated as a function of dopant density and temperature in boron-doped silicon for $10^{13} \leq N_A \leq 3 \times 10^{18}$ cm^{-3} and $100 \leq T \leq 400$ K. The results are compared with experimental data. Figure 1 shows the hole mobility plotted as a function of hole density at 300 K for boron-doped silicon. Curve 1 is the theoretical calculation using eqs (1) through (24). Open circles are hole mobility data published by Thurber *et al.* [26] and solid triangles are given by Horn [27]. These results are in excellent agreement with our calculated values. Curves 2 and 3 are reproduced from Wagner [9] and Caughey and Thomas [28], respectively. Note that the calculated mobility values are within 5 percent of the values reported by Wagner for $N_A \leq 10^{17}$ cm^{-3}. However, for $N_A \geq 10^{17}$ cm^{-3}, the calculated values are substantially higher than those of Wagner [9] (e.g., the deviation is 2.2 percent at 10^{17} cm^{-3}, and increases to 22.6 percent at 10^{18} cm^{-3}). To explain this discrepancy, note that Wagner [9] obtained an empirical mobility expression based on measurements of boron-implanted silicon. The amount of boron retained in the silicon was determined by integration of data obtained from incremental sheet resistance and Hall effect measurements on layers which were sectioned by anodic oxidation. A mobility value as a function of boron density was derived which made the integrated dose equal to the implanted dose. This was done with the assumption that all of the boron was electrically active and ionized. This assumption is valid only at low dopant density or at high temperature where full ionization of boron atoms prevails. For example, the theoretical calculations indicate that at 300 K, $N_A^-/N_A = 0.933$ at $N_A = 10^{17}$ cm^{-3}, and $N_A^-/N_A = 0.756$ at $N_A = 10^{18}$ cm^{-3}. Failure to correct this ionization effect at higher dopant density or lower temperature in the mobility calculations results in a large error in mobility values derived from resistivity measurements. Curve 3 was reproduced using the Caughey and Thomas [28] empirical formula fitted to Irvin's mobility curve [29]. This mobility curve is based on data from Hall effect measurements, which give hole density within the uncertainty of the Hall scattering factor and on data from chemical techniques which give total dopant density. The lower mobility values shown in curve 3 as compared to Wagner's may be due in part to the fact that in the region $10^{16} < N_A < 10^{18}$ cm^{-3} Sze and Irvin's [8] mobility curves include data on gallium-doped silicon, which is expected to have a lower mobility value for the same dopant density due to the deeper ionization energy of gallium as compared to boron.

From the above analysis, it is clear that values of carrier mobility calculated from measurements of resistivity and dopant density are correct only if the carrier density is equal to the dopant density. This is not always the case. Figure 2 shows the ratio of ionized and total boron impurity density as a function of boron density for $100 \leq T \leq 400$ K. It is clearly shown in this figure that the deionization of boron impurities is significant for $10^{17} < N_A \leq 3 \times 10^{18}$ cm^{-3} and at low temperatures. In this range the carrier density is equal to the ionized boron density.

The mobility formulas presented in section 2 were used to compute the hole mobility as a function of dopant density and temperature for dopant densities between 10^{13} and 3×10^{18}

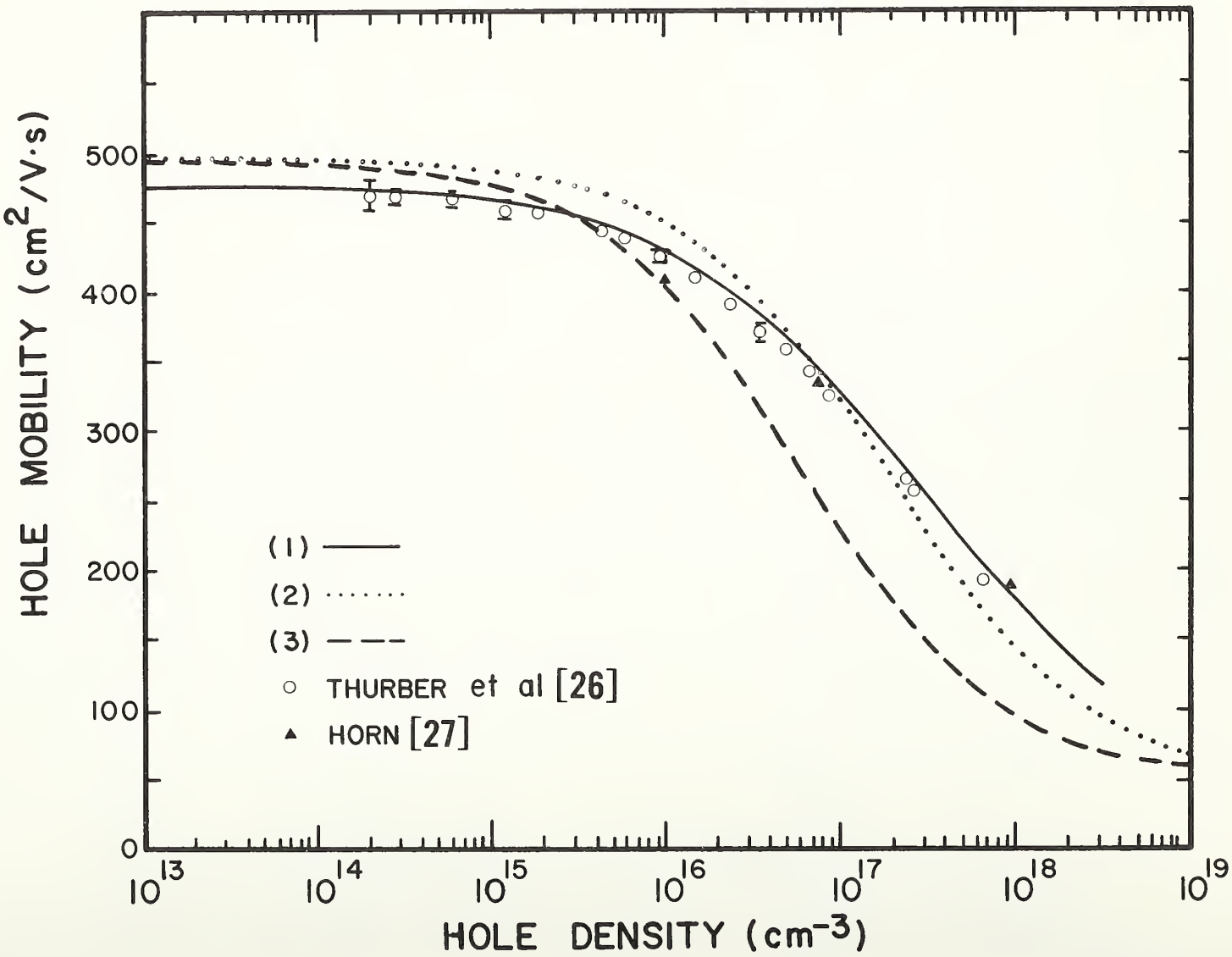

Figure 1. Hole mobility *vs.* hole density for boron-doped silicon at 300 K. Curve 1 is our theoretical calculations, curve 2 is reproduced from Wagner [9], and curve 3 is from Caughey and Thomas [28]. Curves 2 and 3 are plotted by assuming hole density equal to the dopant density, as discussed in the main text.

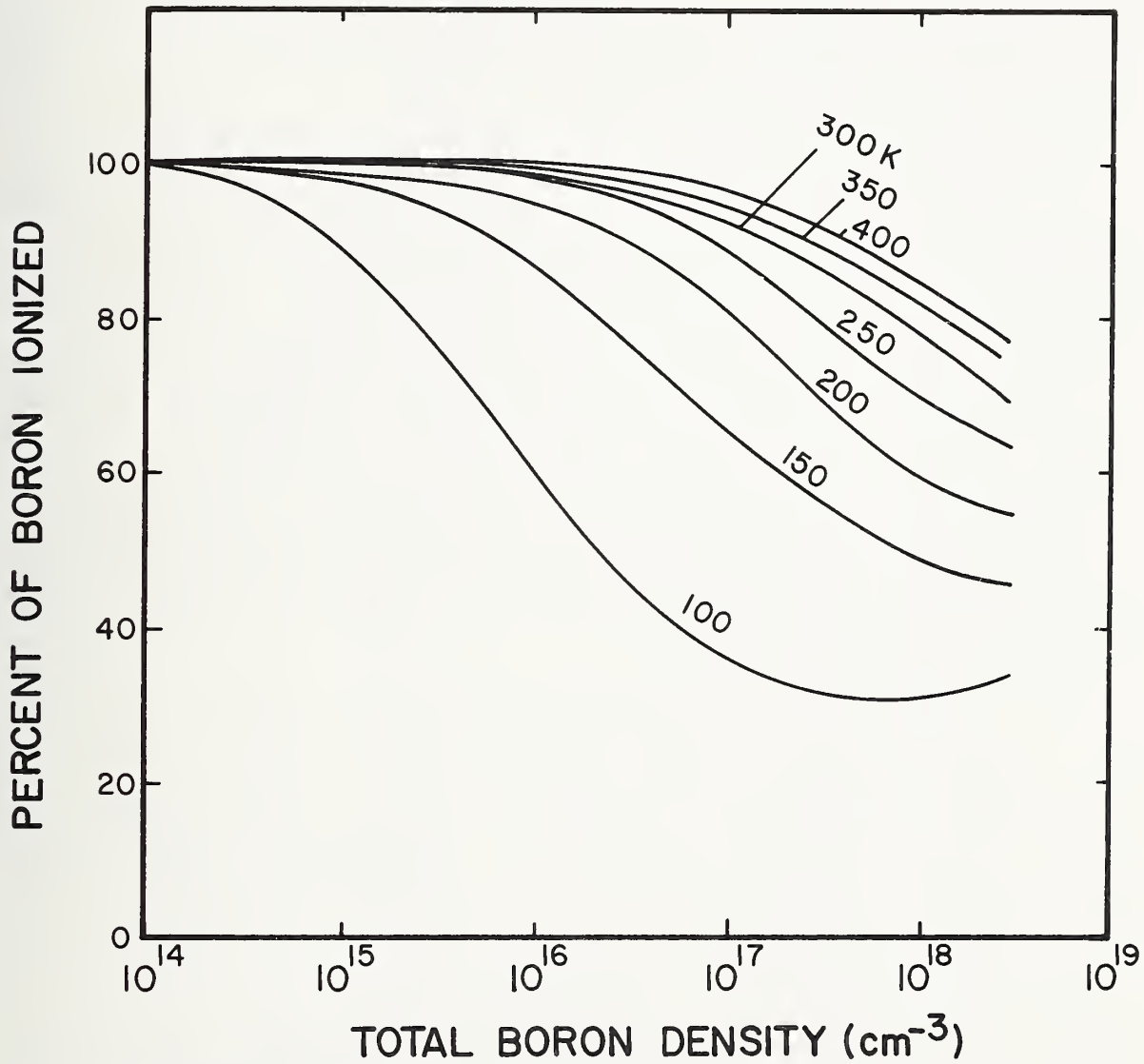

Figure 2. Theoretical calculations of the ratio of ionized and total boron density *vs.* boron density with temperature as a parameter.

cm^{-3} and temperatures between 100 and 400 K. The results are displayed in figures 3 and 4, respectively.

Due to lack of available measured mobility data, comparisons of theory and experiment over the range of dopant density and temperature reported here were unobtainable. In order to verify the adequacy of the theoretical model developed in this work, resistivity measurements were performed on nine boron-doped silicon slices with dopant densities ranging from 4.5×10^{14} to 6×10^{18} cm^{-3} for temperatures between 100 and 400 K, using a planar four-probe square-array test structure [30] as discussed in a previous paper [20]. The results are compared with the theoretical calculations.

The resistivity for boron-doped silicon as calculated from eqs (24) through (29) is shown in figures 5 through 8. Figure 5 shows the plot of resistivity as a function of dopant density of p-type silicon at T = 300 K. The solid line (curve 1) is the theoretical calculation; the solid dots are the experimental data for boron-doped silicon. Note that each experimental data point represents the mean value of resistivity measured on five to seven selected test cells with a maximum variation of resistivity less than 5 percent. The net dopant density in these specimens was determined from measurements of capacitance as a function of voltage on a junction diode test structure near the four-probe square array resistor. Details of this method can be found elsewhere [30]. The dotted curve (curve 3) was reproduced from Irvin's resistivity curve using the Caughey-Thomas formula [28], and the dashed curve (curve 2) is Wagner's for boron-doped silicon [9]. The theoretical calculations agree with Wagner's resistivity data within 6 percent for $N_A \leq 3 \times 10^{18}$ cm^{-3}. Irvin's resistivity values are higher than both Wagner's values and the values calculated and measured here for $N_A > 10^{16}$ cm^{-3}.

Figure 6 shows resistivity as a function of temperature from 100 to 400 K for the eight boron-doped silicon slices with boron density ranging from 4.5×10^{14} to 3.2×10^{18} cm^{-3}. The results show that the agreement between the calculated and measured values is within ±6 percent over the entire range of dopant density and temperature studied. Figure 7 shows the calculated resistivity as a function of dopant density for temperatures between 100 and 400 K at 50-K intervals. Figure 8 displays the calculated resistivity as a function of temperature for dopant density from 10^{13} to 5×10^{18} cm^{-3} in more regular steps.

To illustrate the effect of h-h scattering on the ionized impurity scattering mobility, the mobility reduction factor, γ_{hhI}, is calculated from eq (21). The results, displayed in figure 9, for temperatures between 100 and 400 K, show that h-h scattering increases with increasing dopant density and decreasing temperature, where the deionization effect becomes more prominent.

Finally, it is worth noting that both mobility and resistivity depend more strongly on temperature for the lightly doped case where lattice scattering is dominant, and become less dependent on temperature for dopant density greater than 10^{18} cm^{-3} where neutral impurity scattering prevails. This trend can be seen in figure 4 (mobility) or figure 8 (resistivity). The resistivity and mobility calculations for boron-doped silicon also

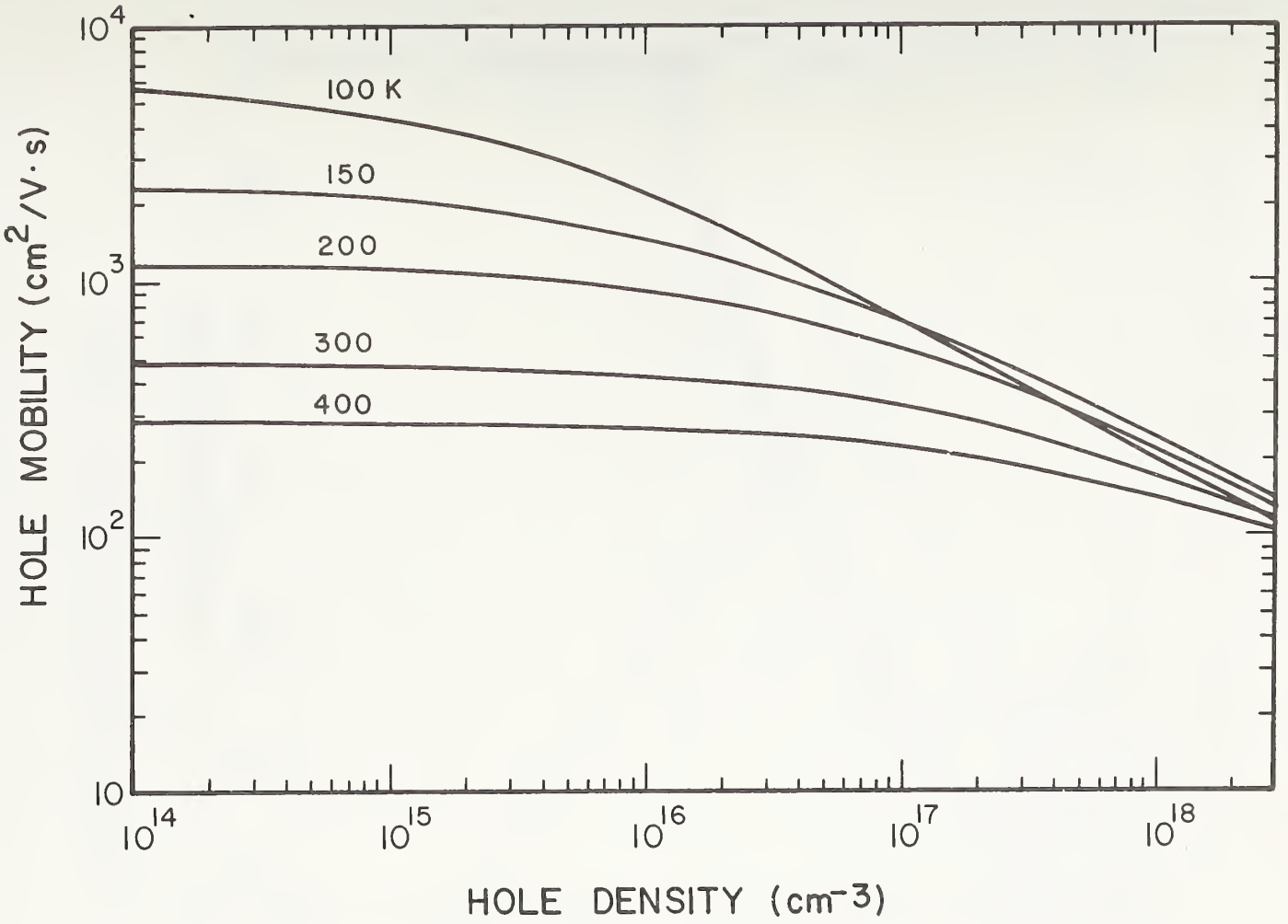

Figure 3. The calculated hole mobility *vs.* hole density for boron-doped silicon with temperature as a parameter.

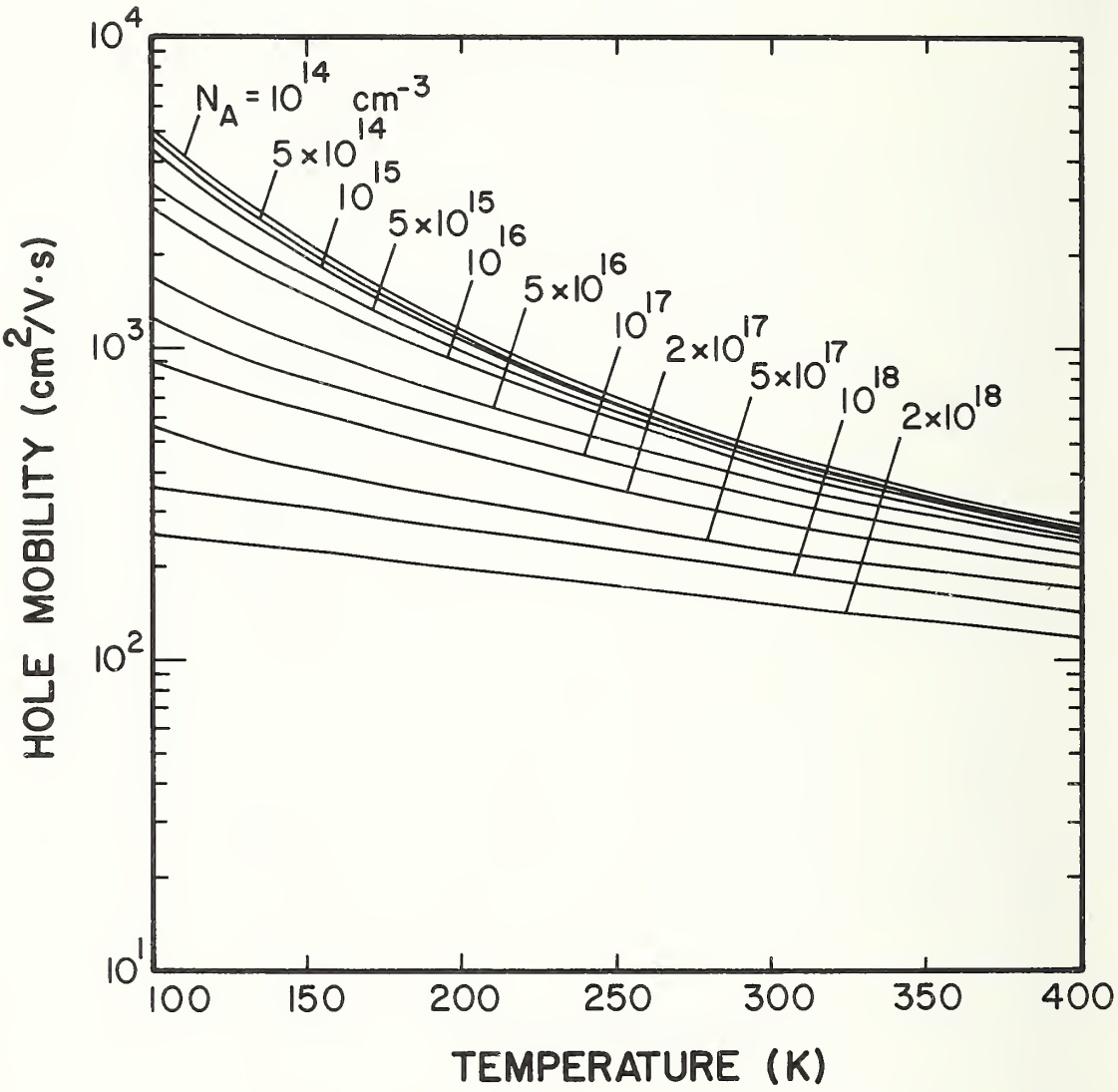

Figure 4. The calculated hole mobility *vs.* temperature for boron-doped silicon with dopant density as a parameter.

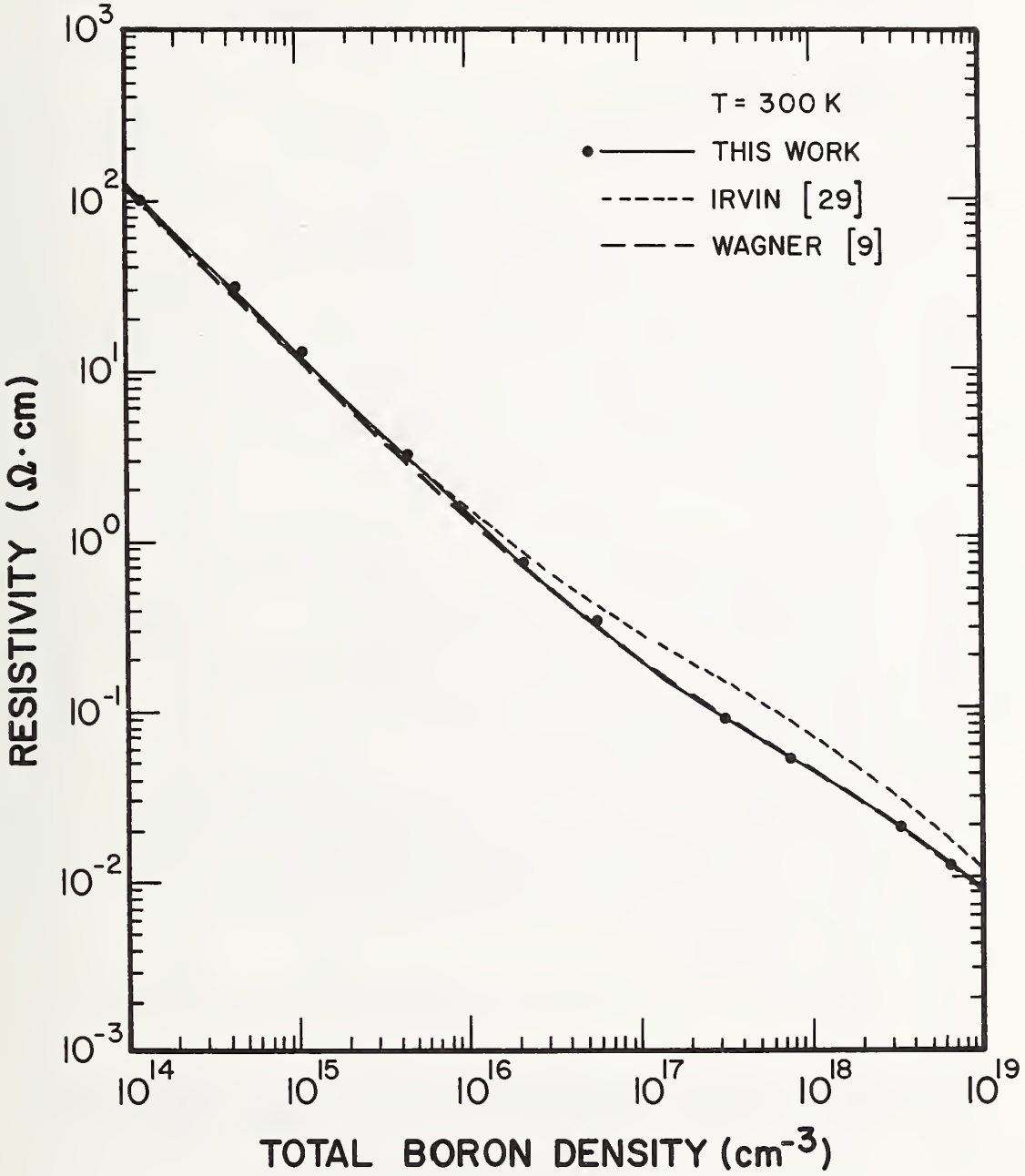

Figure 5. Resistivity *vs.* dopant density for boron-doped silicon at 300 K. Solid line is our theoretical calculation, broken line is from Wagner [9] and dotted line from Irvin [29].

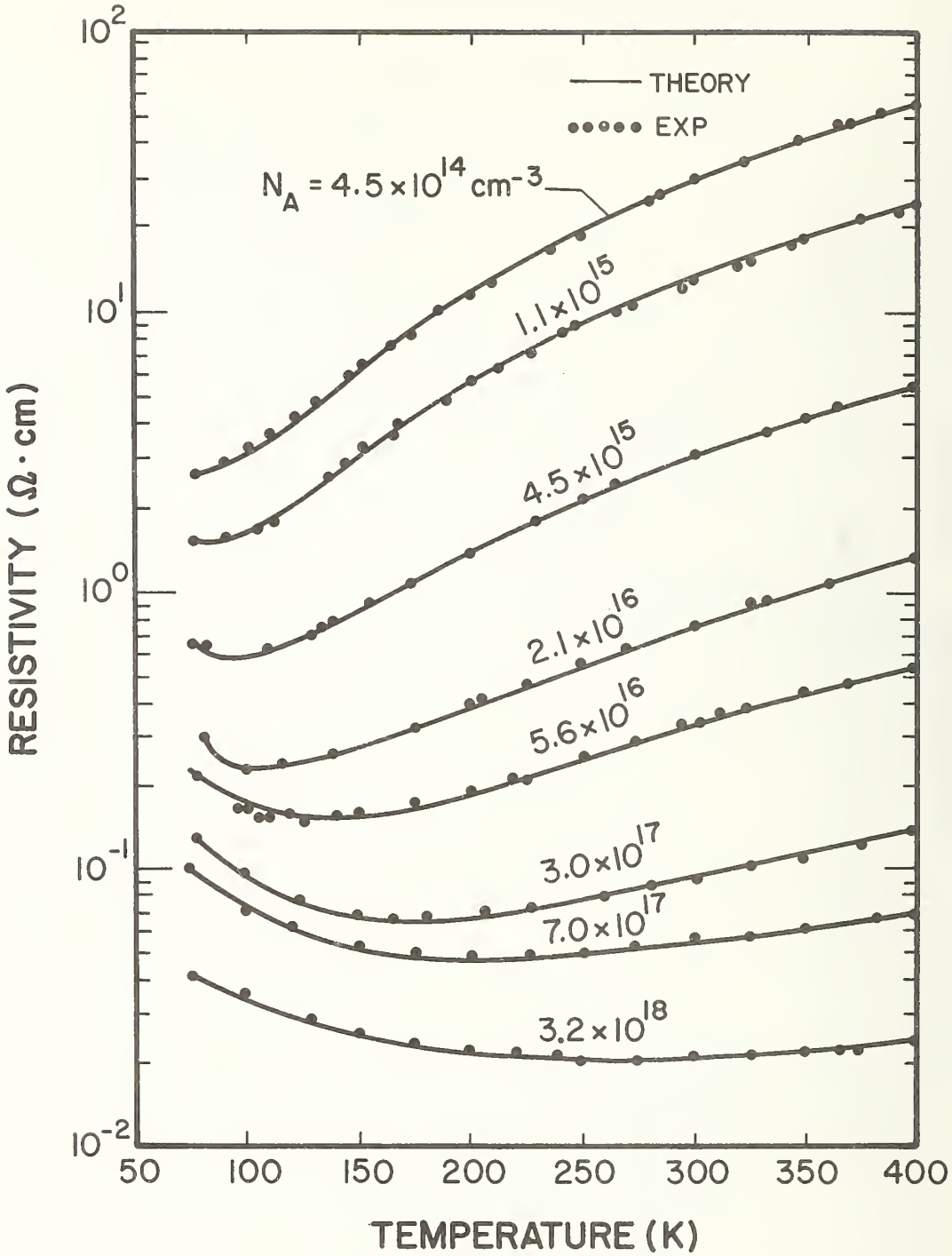

Figure 6. Resistivity *vs.* temperature for eight boron-doped silicon slices. Solid lines are the theoretical calculations and solid dots are the experimental data taken from measurements on the four-probe square-array test structures fabricated on these slices.

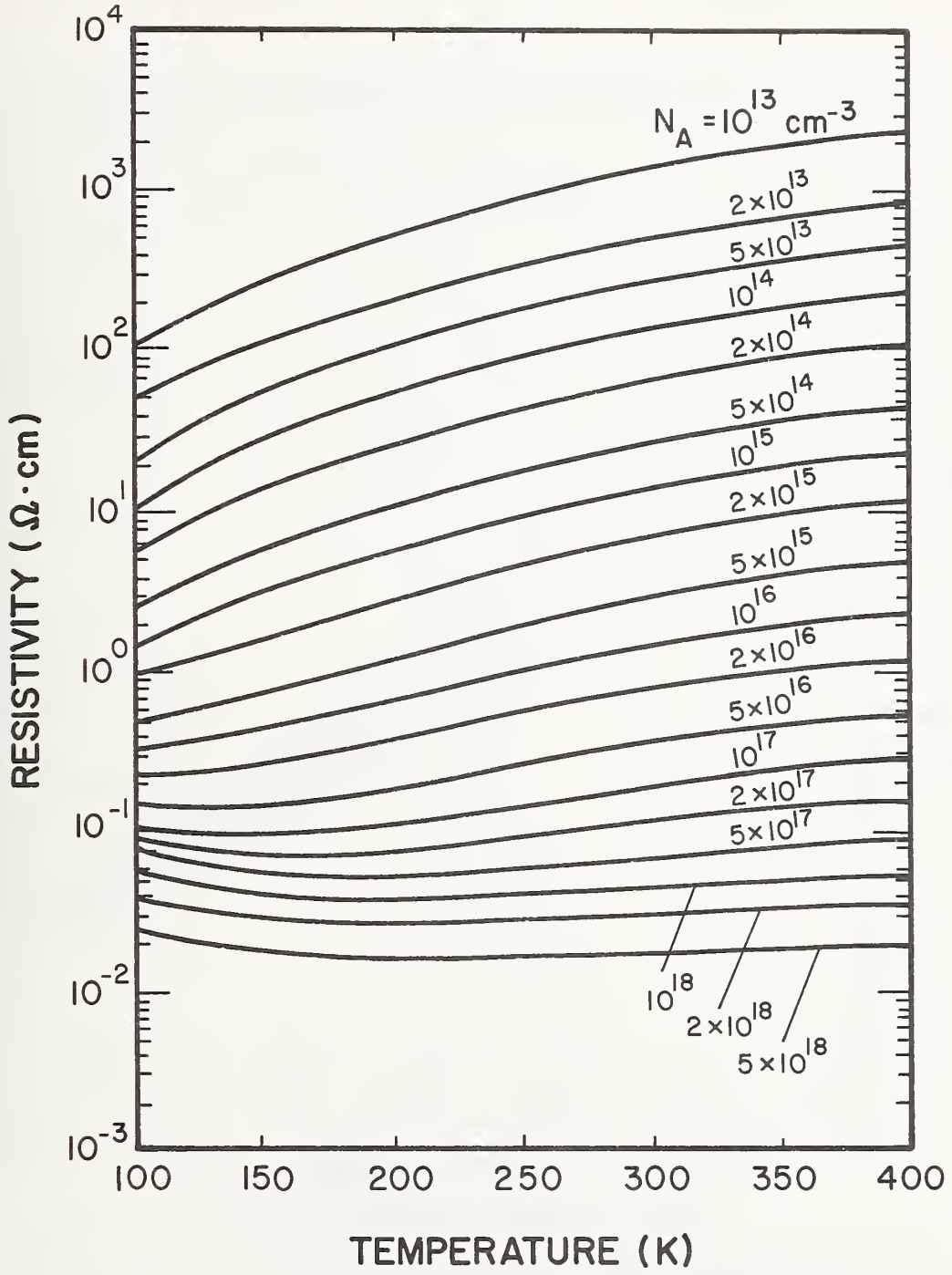

Figure 7. Theoretical calculations of resistivity *vs.* temperature for boron-doped silicon with dopant density as a parameter.

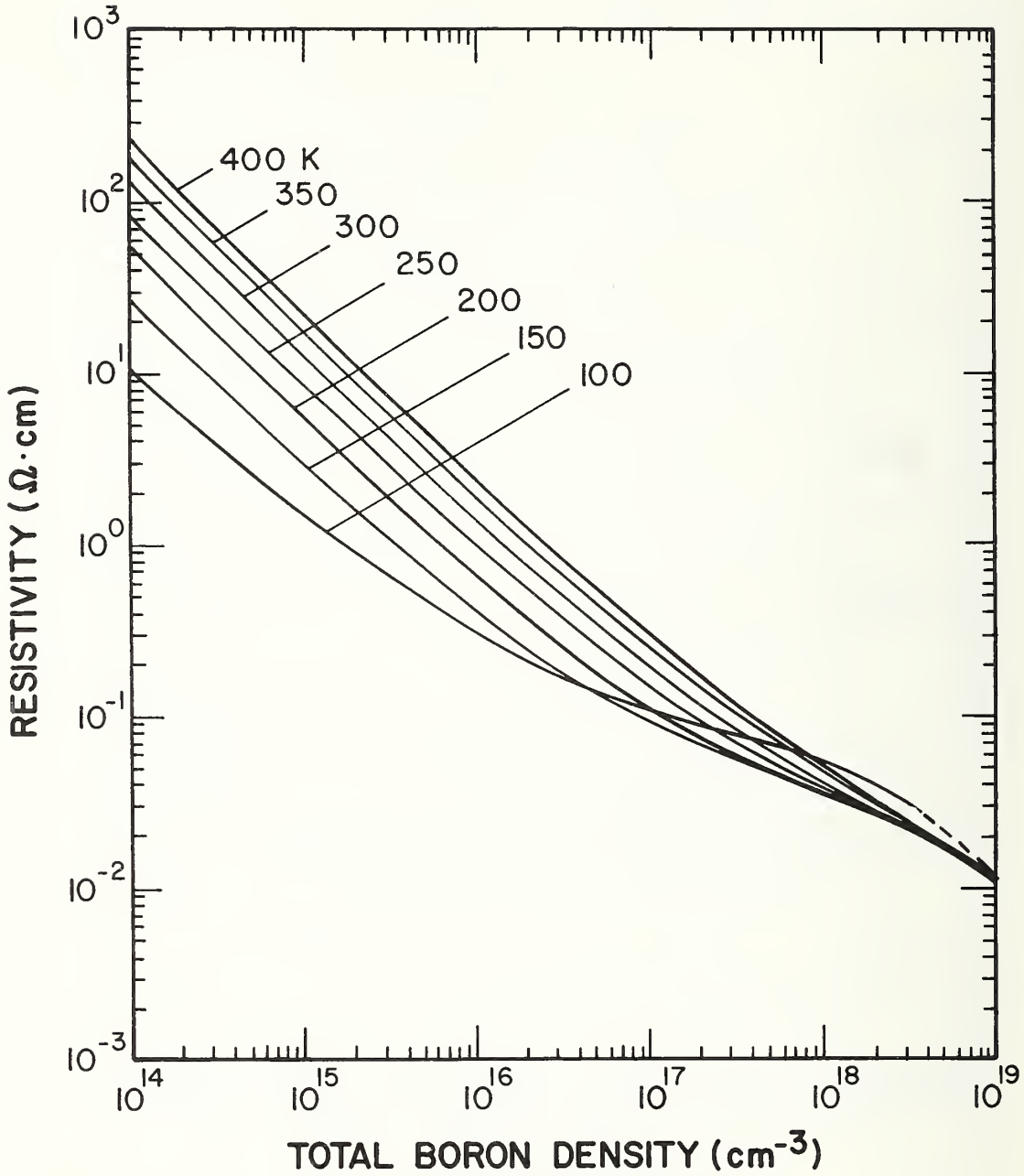

Figure 8. Theoretical calculations of resistivity *vs.* dopant density for boron-doped silicon with temperature as a parameter.

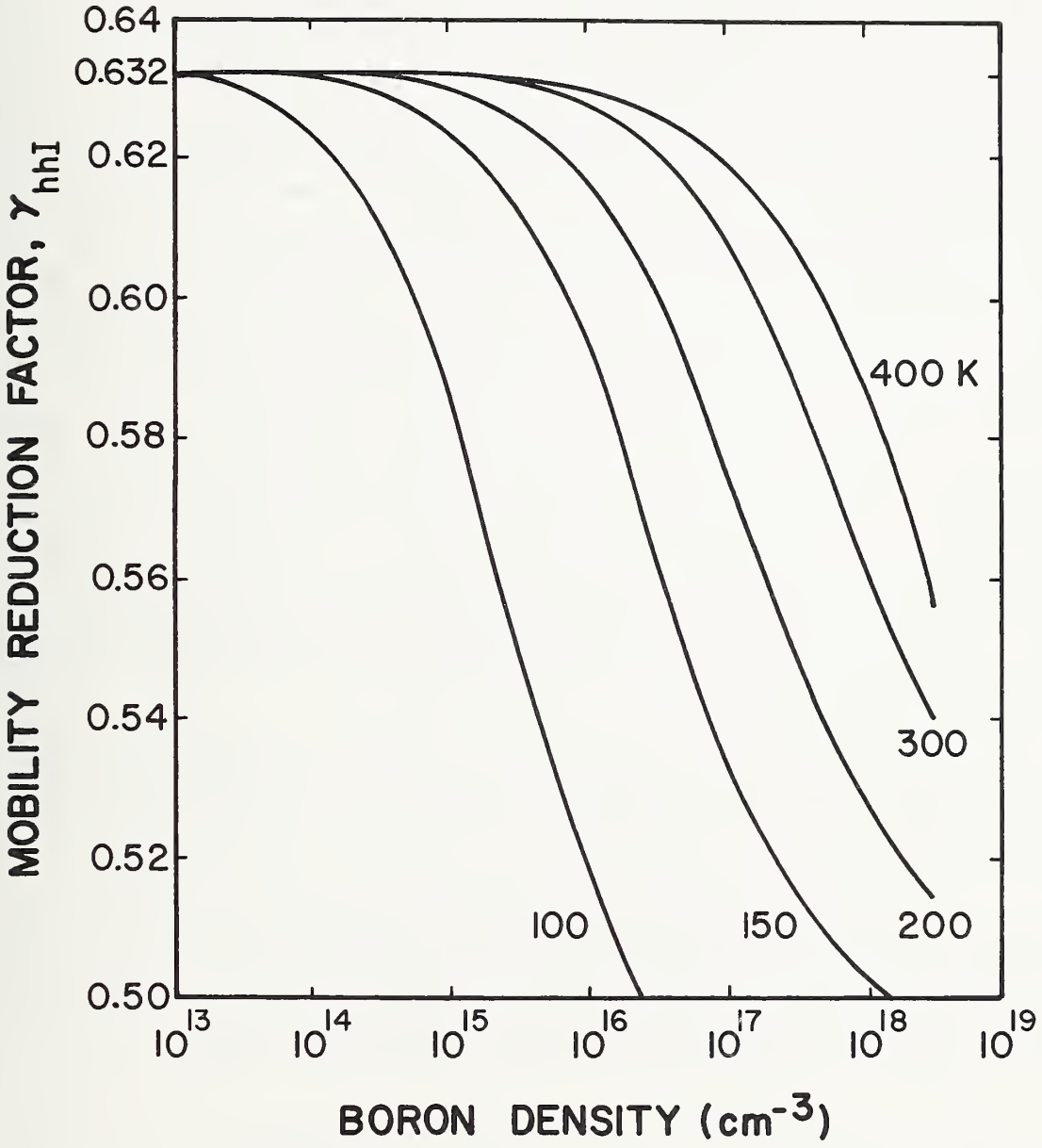

Figure 9. The mobility reduction factor, γ_{hhI}, as a function of dopant density for boron-doped silicon, for $100 \leq T \leq 400$ K, showing the effect of h-h scattering on ionized impurity scattering mobility as is calculated from eq (21).

reveal that contributions from the SO band are negligible for temperatures below 200 K. Using a two-band model in the mobility calculations should not introduce any significant error over the range of dopant densities and temperatures reported here.

4. CONCLUSIONS

Using a three-band model, theoretical expressions have been derived to compute hole mobility and resistivity as functions of dopant density and temperature for boron-doped silicon. In addition to considering contributions from scattering by lattice phonons, ionized impurities, and neutral impurities, the model also takes into account the effect of h-h scattering on both lattice and ionized impurity scattering mobilities. The non-parabolicity of the valence band structure is included in the effective mass calculations.

Resistivity analysis for nine boron-doped silicon samples shows that, for dopant densities less than 3×10^{18} cm^{-3}, agreement between the calculated and measured values of resistivity is within ±6 percent for $100 \leq T \leq 400$ K. A comparison between the calculated mobility values and those of Wagner at 300 K shows that agreement is within ±5 percent for $N_A \leq 1.4 \times 10^{17}$ cm^{-3}, but that differences as large as 27 percent occur at $N_A = 2.5 \times 10^{18}$ cm^{-3}. This discrepancy can be eliminated if the effect of deionization of boron impurity were included in Wagner's calculation. From this study, it was found that the theoretical expressions derived in this work are adequate for mobility and resistivity calculations in boron-doped silicon for $10^{13} \leq N_A \leq 3 \times 10^{18}$ cm^{-3} and $100 \leq T \leq 400$ K. It is important to point out that incorporation of both h-h scattering as well as deionization effects in the mobility and resistivity calculations plays a major role in bringing good agreement between theory and experiment in the range of dopant densities from $5 \times 10^{16} \leq N_A \leq 3 \times 10^{18}$ cm^{-3} for which previous theories failed.

The mobility and resistivity calculations further reveal that contributions from the SO band are negligible for $T < 200$ K. Using a two-band model (i.e., neglecting the SO band contribution) in the mobility calculations should not introduce any noticeable error (i.e., less than 5 percent) over the range of dopant densities and temperatures studied.

Finally, a rigorous formulation for correcting the effect of h-h scattering on lattice and ionized impurity scattering together is needed to further improve our mobility formulations. The extension of the present work to higher dopant densities and lower temperatures requires consideration of additional factors not included in this work.

5. REFERENCES

1. Ottaviani, G., Reggiani, L., Canali, C., Nava, F., and Alberigi-Quaranta, A., Hole Drift Velocity in Silicon, *Phys. Rev. B* 12, 3318-3329 (1975).

2. Costato, M., and Reggiani, L., Ohmic Mobility of Holes in Silicon, *Nuovo Cimento* 68, 64-74 (1970).

3. Morin, F. J., and Maita, J. P., Electrical Properties of Silicon Containing Arsenic and Boron, *Phys. Rev.* 96, 28-35 (1954).

4. Braggins, T. T., Analysis of Carrier Concentration and Mobility in Boron-Doped Silicon, Ph. D. dissertation, University Microfilms International, Ann Arbor, Michigan (1975).

5. Prince, M., Drift Mobility Measurements in N- and P-Type Silicon, *Phys. Rev.* 93, 1204-1206 (1954).

6. Ludwig, G. W., and Watters, R. L., Drift and Conductivity Mobility in Silicon, *Phys. Rev.* 101, 1699-1701 (1956).

7. Sclar, N., Resistivity and Deep Impurity Levels in Silicon at 300 K, *IEEE Trans. Electron Devices* ED-24, 709-712 (1977).

8. Sze, S. M., and Irvin, J. C., Resistivity, Mobility, and Impurity Levels in GaAs, Ge, and Si at 300 K, *Solid-State Electronics* 11, 599-602 (1968).

9. Wagner, S., Diffusion of Boron from Shallow Ion Implants in Silicon, *J. Electrochem. Soc.* 119, 1570-1576 (1972).

10. Tsao, K. Y., and Sah, C. T., Temperature Dependence of Resistivity and Hole Conductivity Mobility in P-Type Silicon, *Solid-State Electronics* 19, 949-953 (1976).

11. Brown, D. M., and Bray, R., Analysis of Lattice and Ionized Impurity Scattering in p-type Germanium, *Phys. Rev.* 127, 1593-1602 (1962).

12. Barber, H. D., Effective Mass and Intrinsic Concentration in Silicon, *Solid-State Electronics* 10, 1039-1051 (1967).

13. Kane, E. O., Energy Band Structure in p-type Germanium and Silicon, *J. Phys. Chem. Solids* 1, 82-99 (1956).

14. Bir, G. H., Normantas, E., and Pikus, G. E., Galvanomagnetic Effects in Semiconductors With Degenerate Zones, *Soviet Phys. Solid-State* 4, 867-877 (1962).

15. Brooks, H., Theory of the Electrical Properties of Germanium and Silicon, *Advances in Electronics and Electron Physics*, L. Marton, Ed., vol. 7, pp. 85-182 (Academic Press, New York, 1955).

16. Herring C., Transport Properties of a Many-Valley Semiconductor, *Bell Syst. Tech. J.* 34, 237-290 (1955).

17. Conwell, E., and Weisskopf, V. F., Ionized Impurity Scattering in Semiconductors, *Phys. Rev.* 77, 388-390 (1950).

18. Sclar, N., Neutral Impurity Scattering in Semiconductors, *Phys. Rev.* 104, 1559-1561 (1956).

19. Erginsoy, C., Neutral Impurity Scattering in Semiconductors, *Phys. Rev.* 79, 1013-1014 (1950).

20. Li, S. S., and Thurber, W. R., The Dopant Density and Temperature Dependence of Hole Density and Resistivity in n-type Silicon, *Solid-State Electronics* 20, 609-616 (1977). See also S. S. Li, *Semiconductor Measurement Technology:* The Dopant Density and Temperature Dependence of Electron Mobility and Resistivity in N-Type Silicon, NBS Special Publication 400-33 (1977).

21. Luong, M., and Shaw, A. W., Quantum Transport Theory of Impurity Scattering-Limited Mobility in N-Type Semiconductors Including Electron-Electron Scattering, *Phys. Rev. B* 4, 2436-2441 (1971).

22. Debye, P. P., and Conwell, E. M., Electrical Properties of N-Type Germanium, *Phys. Rev.* 93, 693-706 (1954).

23. Li, S. S., The Dopant Density and Temperature Dependence of Hole Mobility and Resistivity in Boron-Doped Silicon, *Solid-State Electronics* 21, 1109-1117 (1978).

24. Pearson, G. L., and Bardeen, J., Electrical Properties of Pure Silicon and Silicon Alloys Containing Boron and Phosphorus, *Phys. Rev.* 75, 865-883 (1949).

25. Penin, N. A., Zhurkin, B. G., and Volkov, B. A., Influence of the Concentration of Donors and Acceptors on the Electrical Conductivity of Heavily Doped n-Type Silicon, *Sov. Phys. Solid-State* 7, 2580-2584 (1966).

26. Thurber, W. R., Mattis, R. L., and Liu, Y. M., Resistivity-Dopant Density Relationship for Silicon, *Semiconductor Characterization Techniques*, Proceedings Volume 78-3, P. A. Barnes and G. A. Rozgonyi, Eds., pp. 81-92 (ECS, Princeton, New Jersey, 1978).

27. Horn, F. H., Densitometric and Electrical Investigation of Boron in Silicon, *Phys. Rev.* 97, 1521-1525 (1955).

28. Caughey, D. M., and Thomas, R. E., Carrier Mobilities in Silicon Empirically Related to Doping and Field, *Proc. IEEE* 55, 2192-2193 (1967).

29. Irvin, J. C., Resistivity of Bulk Silicon and of Diffused Layers in Silicon, *Bell System Tech. J.* 41, 387-410 (1962).

30. Buehler, M. G., *Semiconductor Measurement Technology:* Microelectronic Test Pattern NBS-3 for Evaluating the Resistivity-Dopant Density Relationship of Silicon, NBS Special Publication 400-22 (1976); Buehler, M. G., and Thurber, W. R., A Planar Four Probe Test Structure for Measuring Bulk Resistivity, *IEEE Trans. Electron Devices* ED-23, 968-974 (1976).

APPENDIX

TEMPERATURE DEPENDENCE OF THE COMBINED DENSITY OF STATES, CONDUCTIVITY, AND HALL EFFECTIVE MASS OF HOLES IN *P*-TYPE SILICON*

by

L. C. Linares and S. S. Li

Department of Electrical Engineering
University of Florida
Gainesville, FL 32611

ABSTRACT

A derivation involving the use of the Boltzmann transport theory is applied to obtain expressions for the density-of-states effective mass, m_D^*, the conductivity effective mass, m_C^*, and the Hall effective mass, m_H^*, of holes in *p*-type silicon. The valence band model as determined by Kane consists of a parabolic heavy-hole band, a non-parabolic light-hole band, and the split-off (SO) band. Values of effective mass calculated from this model reveal the temperature and dopant density dependence of the effective mass due to the anisotropic, non-parabolic shape of the bands.

Calculations are carried out for dopant densities from 10^{14} to 10^{18} cm^{-3} and for temperatures from 50 to 400 K for boron-doped silicon. Conductivity effective mass increases from a value of 0.268 m_o at 50 K to a value of 0.490 m_o at 400 K, while Hall effective mass increases from 0.182 m_o at 50 K to 0.526 m_o at 400 K. For temperatures above 100 K, m_C^* shows little change with dopant density, but m_H^* varies by as much as 35 percent over the range of dopant densities considered.

1. INTRODUCTION

The interpretation of transport properties in silicon and the modeling of silicon junction devices depend on an accurate knowledge of values of effective mass. The complex valence band structure of silicon leads to difficulties in the study of transport properties of holes in this material. Thus, the development of a model incorporating the non-parabolic and anisotropic nature of the band into a single parameter, the combined hole effective mass, would greatly simplify the study of mobility, resistivity, and the Hall effect in silicon. This is a reasonable procedure for including the band non-parabolicity in calculations of relaxation time, and has been applied effectively by Radcliffe [A-1] to study acoustic phonon scattering, and by Barrie [A-2] to study optical phonon and impurity scattering in non-parabolic bands [A-3]. It is the purpose of this paper to derive such a theoretical model for hole effective mass calculations in silicon.

---

* This research was supported in part by the Advanced Research Project Agency Order No. 2397 through the National Bureau of Standards' Semiconductor Technology Program Contract No. 7-35741 and in part by the National Science Foundation Grant No. ENG 72-81828.

Lax and Mavroides [A-4] have derived expressions for density-of-states effective masses m^*_{D1} and m^*_{D2} for the heavy-hole band and the light-hole band, respectively, which lead to the generally accepted and quoted value, $m^*_D = 0.591\ m_o$. This value, however, can only be considered applicable at 4.2 K, where $m^*_{D1} = 0.537\ m_o$ and $m^*_{D2} = 0.153\ m_o$. From the published experimental data it is noted that both electron and hole effective masses are dependent on temperature and dopant density [A-5, A-6]. Below 50 K, hole effective mass remains constant as indicated in high frequency magnetoconductivity experiments [A-7]. However, at higher temperatures and for higher acceptor impurity densities two mechanisms are responsible for the temperature dependence of the effective mass: the thermal expansion of the lattice and the explicit effect of temperature. The effect of the thermal expansion can be estimated from the stress dependence of the effective mass [A-8], and has been shown to be negligible [A-5, A-9]. The explicit temperature effect, however, is of great importance. It consists of the temperature variation of the Fermi distribution function in a non-parabolic band, the temperature-dependent distribution function of the split-off band, and the temperature variation of the curvature at the band extremum due to the interaction between holes and lattice vibrations.

Following the work of Lax and Mavroides [A-4], but using Fermi-Dirac statistics and a simplified model of the valence band structure for silicon, Barber [A-9] obtained an expression for the density-of-states effective mass, m^*_D, which is temperature and hole density dependent. Barber, however, did not apply the non-parabolic model of the valence band to the study of conductivity or Hall effective mass in *p*-type silicon.

Costato and Reggiani [A-10] also developed expressions for m^*_D and m^*_C, the band conductivity effective mass, which show a variation with temperature, but they neglected the effects of the split-off band and the temperature variation of the band curvature.

In this paper the expressions for density-of-states effective mass, conductivity effective mass, and Hall effective mass of holes are derived based on the following definitions. The density-of-states effective mass, m^*_D, enters in the normalization of the distribution function; the conductivity effective mass, m^*_C, is the mass of a mobile charge carrier under the influence of an external electric field; and the Hall effective mass, m^*_H, is the mass of a mobile charge carrier under the application of external electric and magnetic fields. (The reason for these particular definitions of effective masses is that the primary application of this work is to generate improved theoretical calculations of Hall mobility, resistivity, and conductivity mobility [A-11].) These expressions were used to calculate hole effective masses in *p*-type silicon over a wide range of temperature and dopant density. Since the crystal structure of silicon has cubic symmetry, the ohmic mobility and the low-field Hall coefficient are isotropic. An angular average of the effective masses may be performed taking into account separately the warping of the individual bands so that expressions for m^*_D, m^*_C, and m^*_H of isotropic form can be derived. Values calculated from these expressions differ from one another because of the warping and non-parabolicity, and consequently effective mass in each band depends on temperature and dopant density in its own way.

The valence band structure of silicon is presented in section 2. In section 3 expressions for m_D^*, m_C^*, and m_H^* are derived. In section 4 numerical values of effective mass are analyzed, and in section 5 the validity of the model is examined.

2. THE VALENCE BAND STRUCTURE OF SILICON

The theoretical calculations by Kane [A-12] have established some basic features of the valence band of silicon. It consists of heavy-hole and light-hole bands, degenerate at k = 0, and a third band displaced down in energy at k = 0 by spin orbit coupling.

The heavy-hole band is characterized by holes with an energy-independent, but direction-dependent effective mass. The light-hole band is characterized by holes with an energy- and direction-dependent effective mass. These two bands can be described by the E *vs.* k relationship [A-13]

$$E(k) = \frac{-\hbar^2}{2m_o}\left\{Ak^2 \pm \left[B^2k^4 + C^2(k_x^2k_y^2 + k_x^2k_z^2 + k_y^2k_z^2)\right]^{1/2}\right\}, \qquad \text{(A-1)}$$

where A, B, and C are the experimentally determined inverse mass band parameters, $k = (k_x^2 + k_y^2 + k_z^2)^{1/2}$, and the upper sign is associated with the holes in the light-hole band, while the lower sign is associated with the holes in the heavy-hole band. Values of A, B, and C are obtained by cyclotron resonance measurements at 4 K [A-6, A-14].

Although warped, the bands are parabolic for small values of k. However, for larger values of k, the bands become non-parabolic, and along the <100> and <111> directions the heavy-and light-hole bands are parallel over most of the Brillouin zone. This situation, however, is not strictly valid for general directions [A-6]. The assumption of overall parallelism while questionable in III-V compounds, is reasonable in the case of Ge and Si [A-15, A-16]. The split-off band is separated at k = 0 by an energy Δ = 0.044 eV [A-17], and is characterized by an effective mass which is independent of energy and direction. If the anisotrophy is small, the square root in eq (A-1) may be expanded [A-4] and the energy surfaces may be expressed by

$$E = E_V - \frac{\hbar^2k^2}{2m_o}(A \pm B')j(\theta,\phi), \qquad \text{(A-2}$$

where $B' = (B^2 + C^2/6)^{1/2}$, $\gamma = \mp C^2/2B'(A\pm B')$, θ and ϕ are the spherical coordinates, E_V is the top of the valence band, and

$$j(\theta,\phi) = 1 + \frac{1}{2}\gamma\left[\sin^4\theta(\cos^4\phi + \sin^4\phi) + \cos^4\theta - 2/3\right]. \qquad \text{(A-2a)}$$

Following the work of Barber [A-9], we have used the simplified model of the band structure illustrated in figure A1. In this model the heavy-hole band is considered parabolic and thus the mass m_1^* is a constant, equal to its value at 4.2 K. For energies within 0.02 eV the light-hole band is considered parabolic with a constant slope corresponding to the value of m_2^* at 4.2 K. For higher energies the light-hole band is assumed to take on approximately the same slope as that of the heavy-hole band, but remains separated from the heavy-hole band by $\Delta/3$ eV [A-12]. The extrapolation of these two constants creates the kink in the light-hole band at 0.02 eV. Because of the change in slope, the light-hole band has

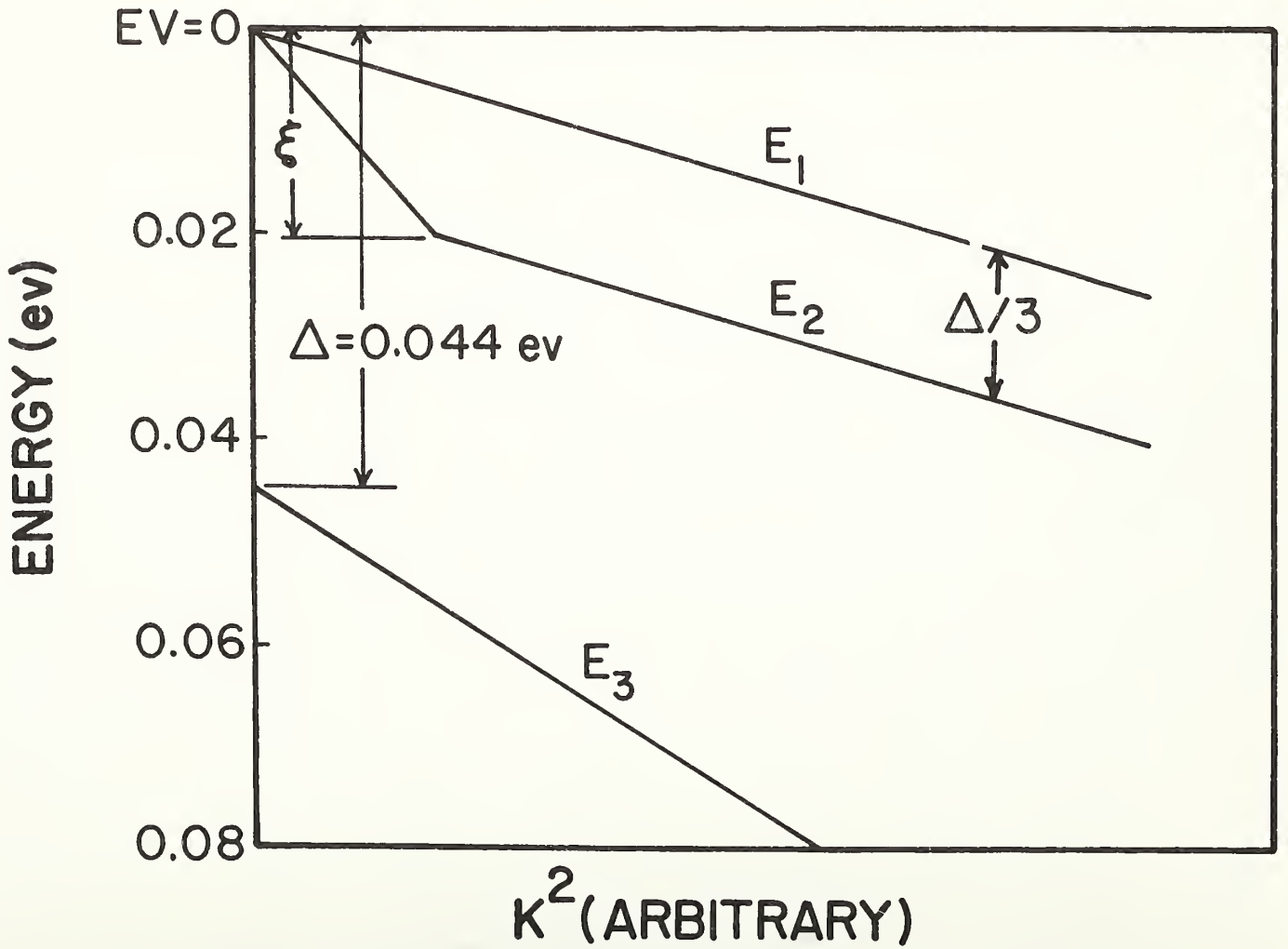

Figure A1. Simplified valence band structure of silicon based on Kane's [A-12] calculations and measured properties of the valence band (after Barber [A-9])

an energy-varying effective mass and in general can only be described in terms of partial Fermi-Dirac integrals [A-9]. Although the split-off band is parabolically disturbed, the apparent effective mass at the top of the valence band is a function of temperature due to the energy displacement at k = 0. Theoretical and experimental studies [A-18, A-19] have shown that at high temperatures the heavy-hole band is not parabolic and thus m_1^* is not energy- and temperature-independent. However, within the range of temperatures considered here, the assumption of parabolicity for the heavy-hole band based on Kane's model [A-12] is reasonable. Other studies [A-20, A-21] support the validity of this model for the valence band of silicon.

3. EFFECTIVE MASS FORMULATION

In the case of spherically symmetric energy surfaces, all of the carriers respond in the same way to a given set of applied forces. The effective mass is a scalar and thus has the same value for the Hall effect, conductivity, and density-of-states masses. For non-spherical energy surfaces, however, this is not the case. The mixed response of carriers to a set of applied forces is reflected in differences between the different kinds of effective masses. The density-of-states effective mass, m_{Di}^*, is defined from the relationship

$$P_i = \frac{4}{\sqrt{\pi}} \left[\frac{2\pi k_o T\, m_{Di}^*}{h^2} \right]^{3/2} \cdot F_{1/2}(\eta) , \qquad \text{(A-3a)}$$

where $\eta = \frac{E_v - E_F}{k_o T}$, E_v is the top of the valence band and E_F is the Fermi-level, k_o is the Boltzman constant, $F_{1/2}(\eta) = \int_o^\infty \frac{\varepsilon^{1/2}\, d\varepsilon}{1+\exp(\varepsilon-\eta)}$, $\varepsilon = \frac{E_v - E}{k_o T}$ and i = 1 or 2 refers to the heavy-hole and light-hole bands, respectively. For the split-off band, the density-of-states effective mass, m_{D3}^*, is defined by

$$P_3 = \frac{4}{\sqrt{\pi}} \left[\frac{2\pi\, m_{D3}^*\, k_o T}{h^2} \right]^{3/2} \cdot F_{1/2}(\eta_2) , \qquad \text{(A-3b)}$$

where $\eta_2 = \eta - \Delta/k_o T$.

The electric current density in the presence of electric and magnetic fields can be expressed by [A-4],

$$J_j = \sigma_C E_j + \sigma_H E_j H_\ell + \sigma_R E_j H_\ell H_m + \cdots , \qquad \text{(A-4)}$$

where E_j, H_ℓ, H_m are the electrical and magnetic field components and the σ's represent single-energy-surface conductivity coefficients. The first coefficient in eq (A-4) is the zero-magnetic field electrical conductivity, and the second coefficient is associated with the non-directional Hall effect. We use σ_C to define the conductivity effective mass, m_{Ci}^*, by the relationship

$$\sigma_{Ci} = P_i \frac{q^2 \langle \tau_i \rangle}{m_{Ci}^*} , \qquad \text{(A-5)}$$

and σ_H to define the Hall mobility effective mass by means of [A-22]

$$\sigma_{Hi} = P_i \frac{q^3 \langle \tau_i^2 \rangle}{(m^*_{Hi})^2} . \tag{A-6}$$

Equations (A-5) and (A-6) apply both to the parabolic and non-parabolic cases. Both effective mass and scattering relaxation time are energy dependent and are being averaged over energy and direction, but we have separated them in order to solve for effective mass in terms of relaxation time. By defining P_i as in (A-3), we model the bands as parabolic with m^*_{Di}, m^*_{Ci}, and m^*_{Hi} containing information relative to the true, non-parabolic shape of the bands. To obtain m^*_{Di} [A-4, A-9], the number of holes in each band is computed from

$$P_i = \frac{1}{4\pi^3} \int f_p(k)\, d^3k , \tag{A-7}$$

where f_p is the Fermi-Dirac distribution function. The conductivity in the direction of an applied electric field may be expressed by [A-22]

$$\sigma_c = \frac{q^2}{4\pi^3 \hbar^2} \int \tau \left(\frac{\partial E}{\partial k}\right)^2 \left[- \frac{\partial f_p(E)}{\partial E} \right] d^3k , \tag{A-8}$$

while the conductivity corresponding to the Hall effect is given by [A-23]

$$\sigma_H = \frac{q^3}{4\pi^3 \hbar^4} \int \tau^2 \frac{\partial f_p(E)}{\partial E} \left[\frac{\partial E}{\partial k}\right]^2 \frac{\partial^2 E}{\partial k^2}\, d^3k . \tag{A-9}$$

Since eqs (A-7) through (A-9) do not use the effective mass, they are valid both for parabolic and non-parabolic band structures.

In order to derive expressions for the effective masses, each warped, non-parabolic band is expressed by eqs (A-7), (A-8), and (A-9). Corresponding parabolic heavy-hole, light-hole, and split-off bands are represented by eqs (A-3), (A-5), and (A-6). Thus, by substituting eq (A-2) into (A-7), (A-8), and (A-9) and equating these to eqs (A-3), (A-5), and (A-6), we can solve for m^*_{Di}, m^*_{Ci}, and m^*_{Hi}. These are discussed separately as follows:

(a) The heavy-hole band

In this band, the effective masses are given by

$$m^*_{Dl} = \frac{m_o}{(A-B')} [f(-\gamma)]^{2/3} , \tag{A-10}$$

$$m^*_{Cl} = \frac{m_o}{(A-B')} \frac{3F_{1/2}(\eta)}{2\phi_{3/2}(\eta)} \frac{f(-\gamma)}{f_1(-\gamma)} , \tag{A-11}$$

and

$$m^*_{Hi} = \frac{m_o}{(A-B')} \left[\frac{{}^3F_{1/2}(\eta)}{2\phi_{3/2}(\eta)} \; \frac{f(-\gamma)}{f_2(-\gamma)} \right]^{1/2} \tag{A-12}$$

where γ is defined in [A-2] by

$$\begin{aligned} f(\gamma) &= (1 + 0.05\gamma + 0.01635\gamma^2 + 0.000908\gamma^3 + \ldots) , \\ f_1(\gamma) &= (1 + 0.01667\gamma + 0.041369\gamma^2 + 0.00090679\gamma^3 + 0.00091959\gamma^4 + \ldots), \\ f_2(\gamma) &= (1 - 0.01667\gamma + 0.017956\gamma^2 - 0.0069857\gamma^3 + 0.0012610\gamma^4 + \ldots), \end{aligned} \tag{A-12a}$$

and

$$\phi_{3/2}(\eta) = \int_0^\infty \frac{\varepsilon^{3/2} \exp(\varepsilon-\eta)\, d\varepsilon}{[1 + \exp(\varepsilon-\eta)]^2} . \tag{A-12b}$$

Since the heavy-hole band was assumed parabolic, the integrals containing τ in eqs (A-7) through (A-9) are identical and can be canceled out. The anisotropic nature of the band is represented by the terms in γ, A, and B'. The temperature dependence is introduced by the use of the Fermi-Dirac distribution function, and is only relevant at high dopant densities.

(b) The light-hole band

In the light-hole band, as modeled by figure A1, the effective masses of holes are obtained in terms of partial Fermi-Dirac integrals [A-9].

Thus,

$$(m^*_{D2})^{3/2} = \frac{m_o^{3/2}}{F_{1/2}(\eta)} \left\{ \frac{f(+\gamma)}{(A+B')^{3/2}} \int_0^{\zeta/k_oT} \frac{\varepsilon^{1/2}\, d\varepsilon}{1+\exp(\varepsilon-\eta)} + \frac{f(-\gamma)}{(A-B')^{3/2}} \int_{\zeta/k_oT}^\infty \frac{\varepsilon_1^{1/2}\, d\varepsilon_1}{1+\exp(\varepsilon_1-\eta_1)} \right\} , \tag{A-13}$$

$$m^*_{C2} = \frac{3m_o\langle\tau_2\rangle}{2} \; \frac{\dfrac{f(+\gamma)}{(A+B')^{3/2}} \displaystyle\int_0^{\zeta/k_oT} \frac{\varepsilon^{1/2}\, d\varepsilon}{1+\exp(\varepsilon-\eta)} + \frac{f(-\gamma)}{(A-B')^{3/2}} \int_{\zeta/k_oT}^\infty \frac{\varepsilon_1^{1/2} d\varepsilon_1}{1+\exp(\varepsilon_1-\eta_1)}}{\dfrac{f_1(+\gamma)}{(A+B')^{1/2}} \displaystyle\int_0^{\zeta/k_oT} \frac{\tau_2\varepsilon^{3/2}\exp(\varepsilon-\eta)\, d\varepsilon}{[1+\exp(\varepsilon-\eta)]^2} + \frac{f_1(-\gamma)}{(A-B')^{1/2}} \int_{\zeta/k_oT}^\infty \frac{\tau_2\varepsilon_1^{3/2}\exp(\varepsilon_1-\eta_1)\, d\varepsilon}{[1+\exp(\varepsilon_1-\eta_1)]^2}} \tag{A-14}$$

and

$$m^*_{H2} = m_o \left[\frac{\frac{3<\tau_2^2>}{2} \left\{ \frac{f(+\gamma)}{(A+B')^{3/2}} \int_0^{\xi/k_oT} \frac{\varepsilon^{1/2}d\varepsilon}{1+\exp(\varepsilon-\eta)} + \frac{f(-\gamma)}{(A-B')^{3/2}} \int_{\zeta/k_oT}^{\infty} \frac{\varepsilon_1^{1/2}d\varepsilon_1}{1+\exp(\varepsilon_1-\eta_1)} \right\}}{(A+B')^{1/2} f_2(+\gamma) \int_0^{\xi/k_oT} \frac{\tau_2^2\varepsilon^{3/2}\exp(\varepsilon-\eta)d\varepsilon}{[1+\exp(\varepsilon-\eta)]^2} + (A-B')^{1/2} f_2(-\gamma) \int_{\zeta/k_oT}^{\infty} \frac{\tau_2^2\varepsilon_1^{3/2}\exp(\varepsilon_1-\eta_1)d\varepsilon_1}{[1+\exp(\varepsilon_1-\eta_1)]^2}} \right]^{-\frac{1}{2}}, \quad \text{(A-15)}$$

where $\varepsilon_1 = \varepsilon - \Delta/3k_oT$, $\zeta = \xi - \Delta/3$, $\eta_1 = \eta - \Delta/3k_oT$, and Δ and ξ are defined in figure A1.

In this case, because eqs (A-7) through (A-9) were expressed in terms of partial Fermi-Dirac integrals and eqs (A-3), (A-5), and (A-6) were expressed in terms of complete Fermi-Dirac integrals, the dependence on τ does not cancel out. Thus, the non-parabolicity of the light-hole band introduces a dependence on the scattering relaxation time.

(c) The split-off band

Although the split-off band is parabolic, the apparent effective mass in this band will also exhibit a temperature dependence due to the energy displacement at k = 0. The energy of a hole in the third band is given by

$$E = E_V - \frac{\hbar^2k^2}{2m_o} A - \Delta , \quad \text{(A-16)}$$

where Δ is the split-off energy (0.044 eV) and A is one of the inverse mass band parameters. Substituting eq (A-16) into eqs (A-7), (A-8), and (A-9), and then equating to eqs (A-3), (A-5), and (A-6) for the split-off band, we obtain

$$m^*_{D3} = \frac{m_o}{A} \quad \text{(A-17)}$$

$$m^*_{C3} = \frac{m_o}{A} \frac{3<\tau_3>F_{1/2}(\eta_2)}{2} \left\{ \int_0^{\infty} \frac{\tau_3\varepsilon_2^{3/2}\exp(\varepsilon_2-\eta_2)d\varepsilon_2}{[1+\exp(\varepsilon_2-\eta_2)]^2} \right\}^{-1}, \quad \text{(A-18)}$$

and

$$m^*_{H3} = \frac{m_o}{A} \left\{ \frac{3<\tau_3>F_{1/2}(\eta_2)}{2} \right\}^{1/2} \left\{ \int_0^{\infty} \frac{\tau_3\varepsilon_2^{3/2}\exp(\varepsilon_2-\eta_2)d\varepsilon_2}{[1+\exp(\varepsilon_2-\eta_2)]^2} \right\}^{-1/2}, \quad \text{(A-19)}$$

where $\varepsilon_2 = \varepsilon - \Delta/k_oT$.

The combined hole density-of-states effective mass can be determined by assuming that the total number of holes in the valence band is equal to the sum of the holes in the individual bands:

$$p = p_1 + p_2 + p_3 ; \quad \text{(A-20)}$$

thus,

$$m_D^* = \left[(m_{D1}^*)^{3/2} + (m_{D2}^*)^{3/2} + (m_{D3}^*)^{3/2} F_{1/2}(\eta_2)/F_{1/2}(\eta) \right]^{2/3} . \quad \text{(A-21)}$$

In the nondegeneracy limit, ($\eta << 1$), $F_{1/2}(\eta_2)/F_{1/2}(\eta) = \exp(-\Delta/k_o T)$. This combined effective mass is defined as the mass corresponding to the density of states of an effective single equivalent parabolic valence band. This concept is useful in calculations where the effective density of states at different temperatures can be calculated from one m_D^*. The explicit temperature variation of the band curvature is included by assuming that the density of states near the band edges varies in a similar manner as the temperature dependence of the energy gap [9]. Thus, $(m_D^*)^{3/2}$ is proportional to E_{G0}/E_G where E_{G0} is the energy gap at 0 K.

To evaluate the total band equivalent conductivity and the Hall effective masses, we assume that, in valence band conduction, the total number of holes in motion is equal to the sum of the holes moving on the separate energy surfaces, and that tnese holes can be modeled as moving on a single spherical energy surface. Thus, the ohmic and the Hall conductivities in the equivalent valence band are given by

$$\sigma_C = \sigma_{C1} + \sigma_{C2} + \sigma_{C3} , \quad \text{(A-22)}$$

and

$$\sigma_H = \sigma_{H1} + \sigma_{H2} + \sigma_{H3} , \quad \text{(A-23)}$$

respectively.

Substituting eqs (A-5) and (A-6) into (A-22) and (A-23), it follows that

$$m_C^* = \left\{ \frac{\langle\tau_1\rangle}{\langle\tau\rangle} \left(\frac{m_{D1}^*}{m_D^*}\right)^{3/2} \frac{1}{m_{C1}^*} + \frac{\langle\tau_2\rangle}{\langle\tau\rangle} \left(\frac{m_{D2}^*}{m_D^*}\right)^{3/2} \frac{1}{m_{C2}^*} + \frac{\langle\tau_3\rangle}{\langle\tau\rangle} \left(\frac{m_{D3}^*}{m_D^*}\right)^{3/2} \frac{\exp(-\Delta/k_o T)}{m_{C3}^*} \right\}^{-1} \quad \text{(A-24)}$$

$$m_H^* = \left\{ \frac{\langle\tau_1^2\rangle}{\langle\tau^2\rangle} \left(\frac{m_{D1}^*}{m_D^*}\right)^{3/2} \frac{1}{m_{H1}^{*2}} + \frac{\langle\tau_2^2\rangle}{\langle\tau^2\rangle} \left(\frac{m_{D2}^*}{m_D^*}\right)^{3/2} \frac{1}{m_{H2}^{*2}} + \frac{\langle\tau_3^2\rangle}{\langle\tau^2\rangle} \left(\frac{m_{D3}^*}{m_D^*}\right)^{3/2} \frac{\exp(-\Delta/k_o T)}{m_{H3}^{*2}} \right\}^{-2} \quad \text{(A-25)}$$

Equations (A-24) and (A-25) are valid for the nondegenerate case.

4. RESULTS

Equations (A-21), (A-24), and (A-25) have been evaluated numerically as a function of temperature and acceptor doping density for p-type silicon. Values of the band parameters, $|A| = 4.27$, $|B| = 0.63$ and $|C| = 4.93$, were determined at 4.2 K by Hensel and Feher [A-6] and Balslev and Lewaetz [A-14]. The scattering relaxation time, τ, was calculated by including lattice, ionized impurity, neutral impurity, and hole-hole scattering mechanisms [A-11]. In the case of acoustic phonon scattering, both interband and intraband transitions were considered. In order to simplify the calculations and maintain tractability, anisotropies in the relaxation time were ignored. A rigorous analysis of the conductivities

for nonisotropic scattering would be extremely difficult to carry out because no relaxation time is expected to exist in the usual sense [A-24].

Figure A2 shows the dependence of m_D^* with temperature in the range from 100 to 400 K. The slight temperature dependence due to the explicit temperature variation of the curvature at the edge of the band results in an effective mass increase of about 5 percent in each band at 400 K. This can be seen in the slope of m_{D1}^*. The temperature dependence due to non-parabolicity is very apparent in the shape of the m_{D2}^* curve.

The temperature dependence of the conductivity effective mass and the Hall effective mass is shown in figures A3 and A4, respectively, for dopant density equal to 10^{14} cm^{-3}. One consequence of the non-parabolicity of the light-hole band is an increase in the combined conductivity effective mass as temperature increases from 50 to 400 K. This happens because with increasing thermal energy $k_o T$, more holes reside in the less parabolic regions of the light-hole band. The results plotted in figure A3 show an increase in m_C^* of about 83 percent in this temperature range. The temperature dependence of m_H^* can be attributed mainly to the non-parabolicity of the light-hole band. In the temperature range from 50 to 400 K, m_H^* increases from 0.182 to 0.526 m_o. The slight temperature dependence of m_{C1}^* and m_{H1}^* is due to the explicit temperature effect and results in increases of 7.7 percent and 3.76 percent in m_{C1}^* and m_{H1}^*, respectively. A larger temperature variation occurs in the case of the split-off band because of the additional effects of the energy displacement at $k = 0$.

Figures A5 and A6 show the variation of m_C^* and m_H^* with dopant density and temperature. For $T \geq 100$ K, m_C^* varies less than 10 percent in the dopant density range from 10^{14} to 10^{18} cm^{-3}. Since the influence of non-parabolicity is reduced in degenerate material [A-19], it follows as shown in figures A5 and A6 that the variation of effective mass with temperature is much stronger at low dopant densities. At lower temperatures there is a much greater change in effective mass due to variations in scattering relaxation time with percentage of ionized impurities.

5. DISCUSSION

The idea of temperature-dependent mass is supported by a number of experimental data. Cardona *et al.* [A-5] found an increase of about 12 percent in optical effective mass between 90 and 300 K in heavily doped *p*-type silicon. Cyclotron-resonance studies conducted by Hensel and Feher [A-6] show that when carrier heating populates deeper regions of the light-hole band, the non-parabolic nature of this band at higher values of k results in an increase in the effective mass of holes.

The model used here in the calculation of hole density-of-states effective mass is identical to that of Barber [A-9], and consequently our results for m_{Di}^* and m_D^* are in excellent agreement with those of Barber [A-9]. We have extended Barber's work to the calculations m_C^* and m_H^* in *p*-type silicon. The increase of m_C^* by 83 percent at 400 K shown in figure A3 is much larger than that reported by Costato and Reggiani (15 percent) [A-10]. Their calculation was done over a similar range of temperatures, and their value at 50 K,

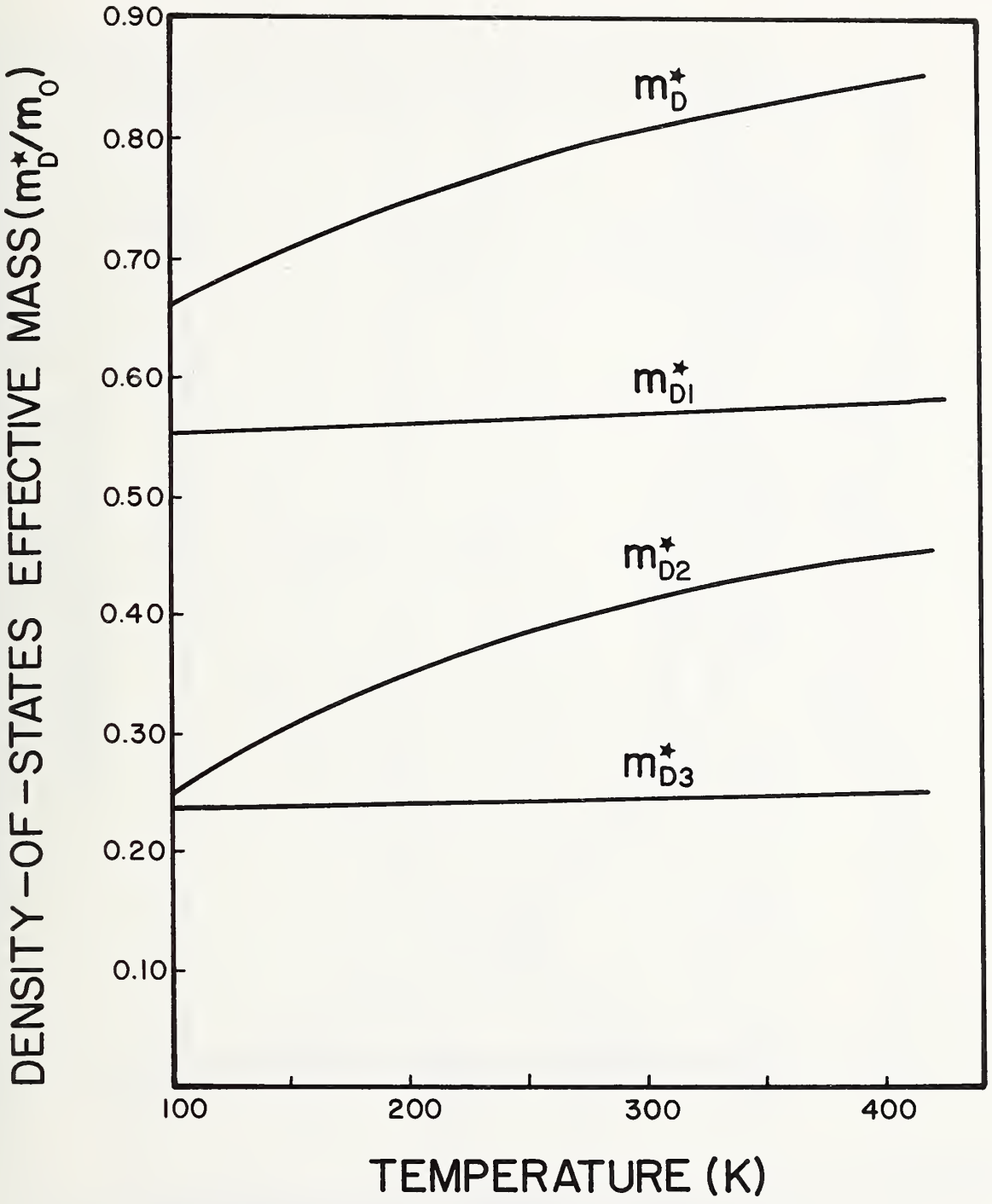

Figure A2. Temperature dependence of the density-of-states effective masses m_{D1}^*, m_{D2}^*, and m_{D3}^* in the individual bands, and the combined density-of-states effective mass m_D^* of holes in silicon. $N_A = 10^{14}$ cm^{-3}. Note that the effective masses have been corrected for the temperature variation of curvature at the edge of the band.

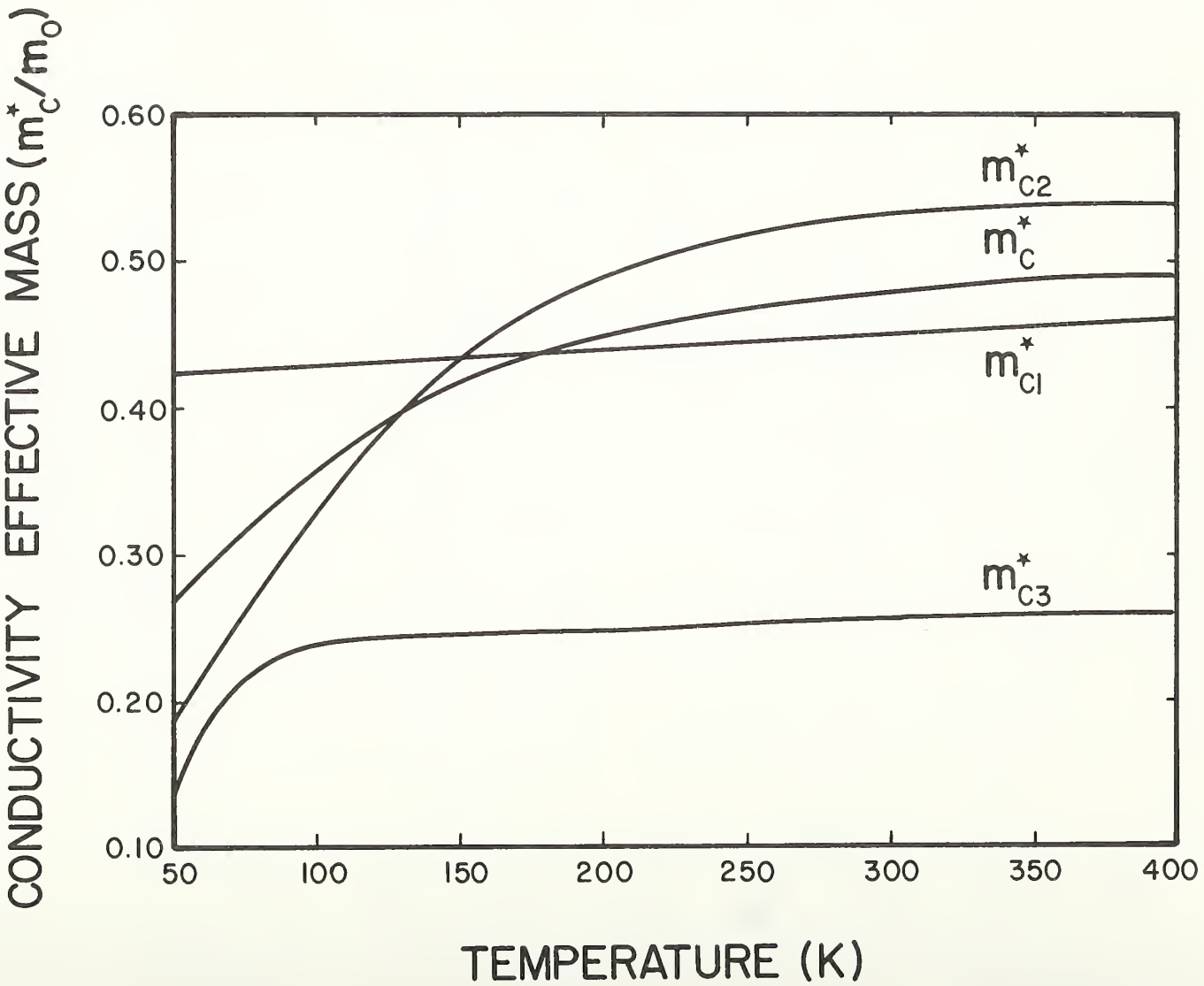

Figure A3. Temperature dependence of the conductivity effective masses m_{C1}^*, m_{C2}^*, and m_{C3}^* in the individual bands, and the combined conductivity effective mass m_C^* of holes in silicon. $N_A = 10^{14}$ cm^{-3}.

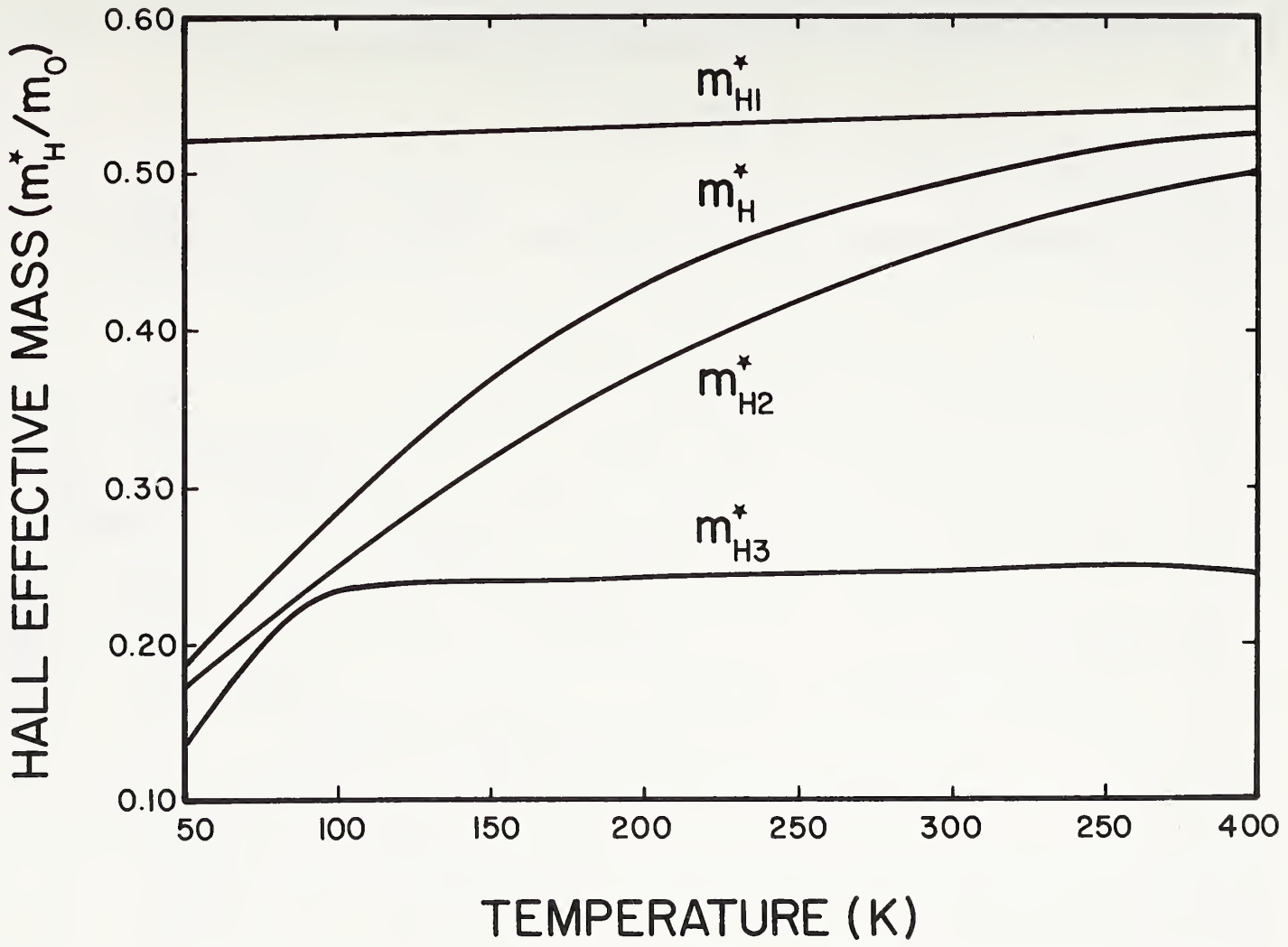

Figure A4. Temperature dependence of the Hall effective masses, m_{H1}^*, m_{H2}^*, and m_{H3}^* in the individual bands, and the combined Hall effective mass m_H^* of holes in silicon. $N_A = 10^{14}$ cm^{-3}.

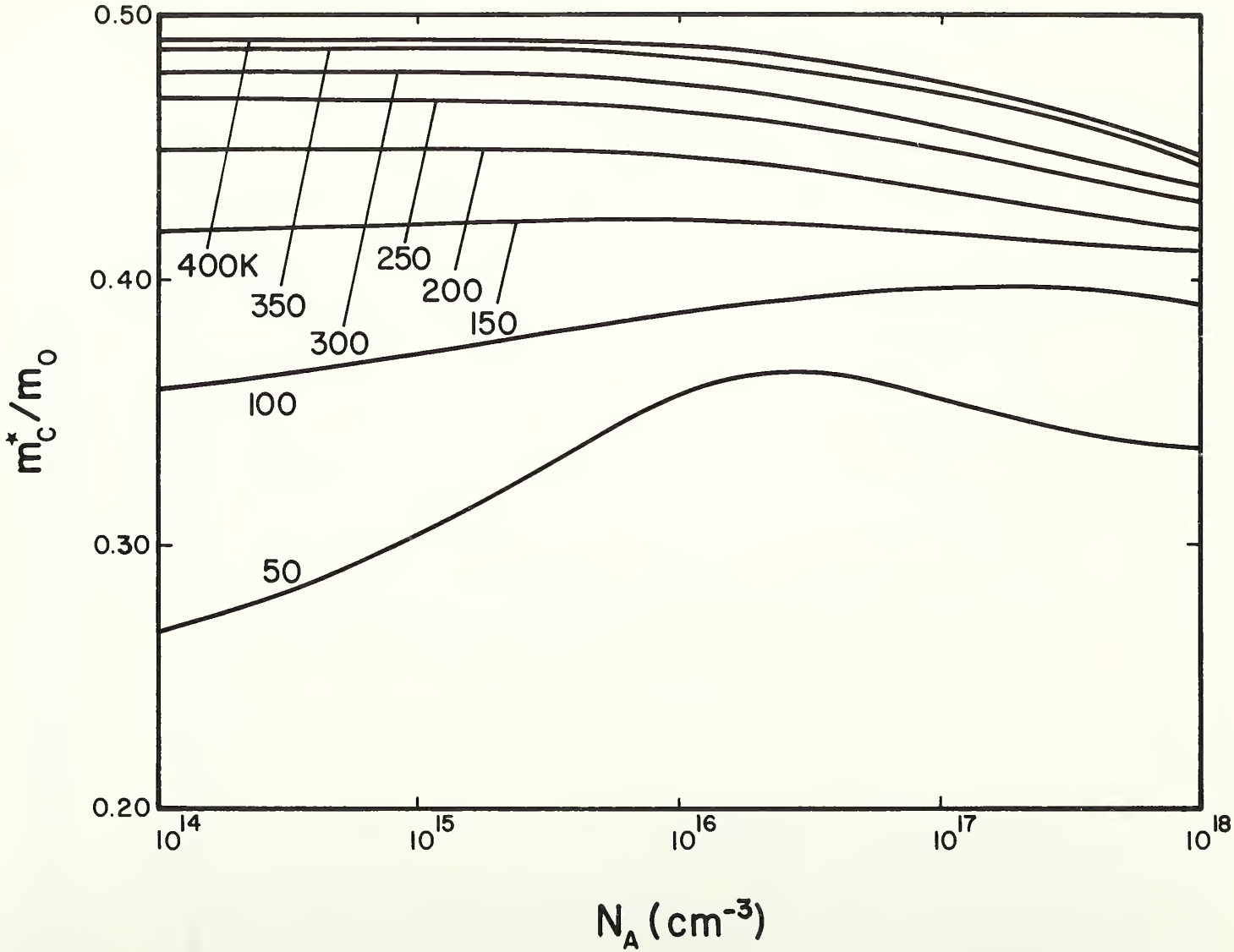

Figure A5. The acceptor density dependence of the combined conductivity effective mass of holes in silicon as a function of temperature.

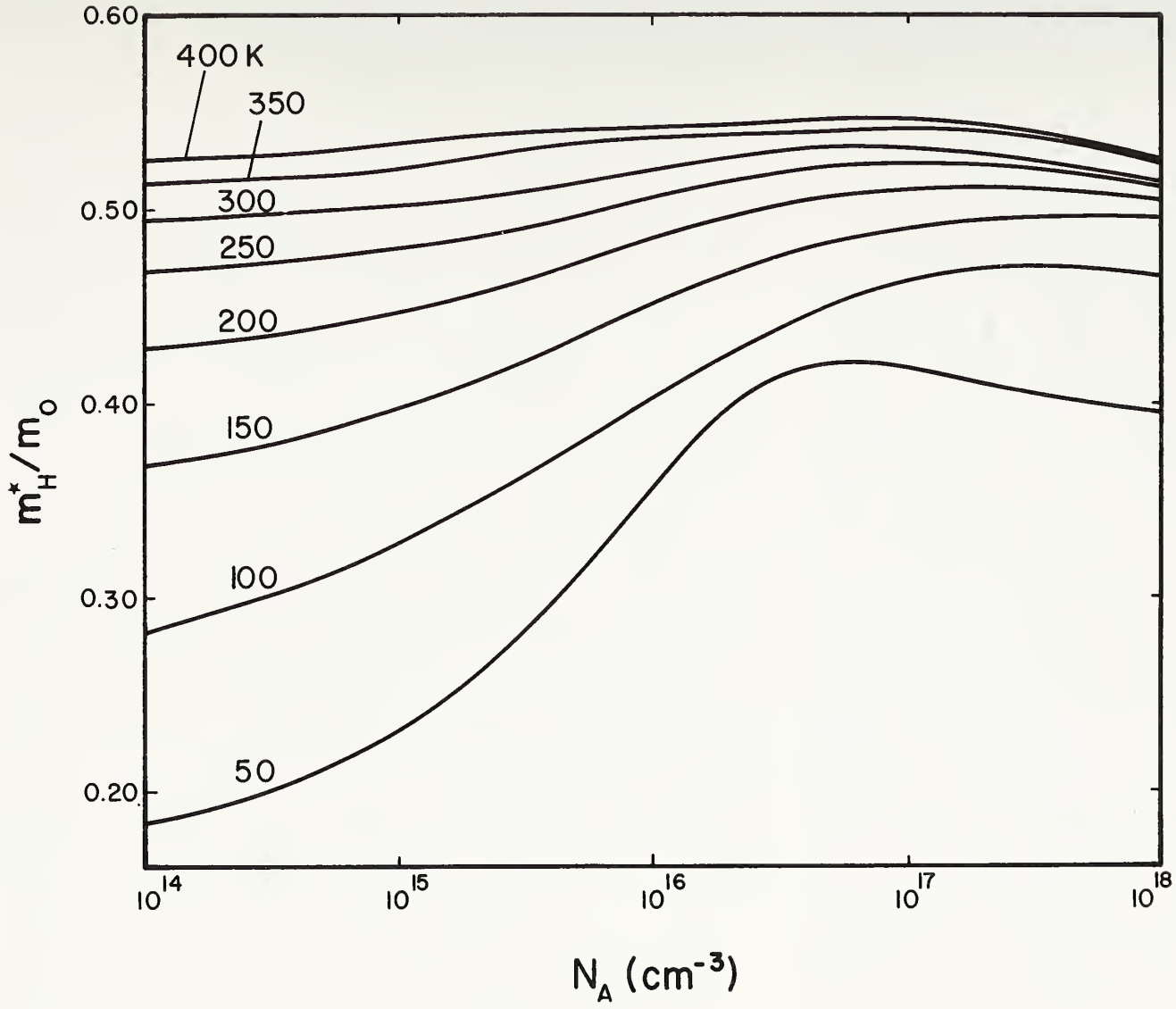

Figure A6. The acceptor density dependence of the combined Hall effective mass of holes in silicon as a function of temperature.

$m_C^* = 0.33\ m_o$, is somewhat higher than our calculated value. The discrepancies between our results and those of Costato and Reggiani are due mainly to the correction of m_D^* for the explicit temperature dependence of the energy gap, the inclusion of the SO band, and the consideration of unequal relaxation times in the three bands. Note that our calculations of effective masses were achieved through more rigorous mathematical derivations, while those of Costato and Reggiani followed a more empirical curve-fitting type of procedure.

The experimental values of density-of-states effective masses of holes in p-type silicon have been published by several authors [A-5, A-6], but very little data can be found for the conductivity and the Hall effective masses, making it difficult to properly assess the value of our calculations. Magneto-kerr effect measurements conducted by Hauge [A-25] indicate that m_C^* could increase by as much as 48 percent in the range of temperatures from 0 to 300 K. This is smaller than our calculated percentage increase in m_C^*, but it is impossible to compare our calculations with Hauge's experimental results, because our effective mass definition was chosen to be mainly applicable to the study of the Hall and conductivity mobility in the low field limit, and this may not apply to the measurements of Hauge [A-25].

From the results of this work, it can be seen that the approximation of a constant effective mass seems to be inadequate to describe transport properties of holes in silicon above 50 K. There is a substantial increase in the effective mass of holes from 50 to 400 K due to the non-parabolicity of the light-hole band, and a smaller, though not negligible, contribution due to the explicit temperature dependence and the effects of the split-off band. The validity of this model for the calculation of density-of-states effective mass has been well established [A-9]. Barber [A-9] has shown that when the temperature-dependent effective masses are substituted into the theoretical expression for intrinsic carrier density in silicon, the agreement with reported measurements of n_i is within the limits of experimental error. Application of this model to theoretical calculation of mobility and resistivity in p-type silicon [A-11] has provided excellent agreement between theoretical and experimental values (resistivity within ±6 percent) over a temperature range from 100 to 400 K and dopant density range from 10^{14} to 3×10^{18} cm^{-3}. This calculation is limited to applications in ohmic mobility and low field Hall effect.

REFERENCES

A-1. Radcliffe, J. M., On Lattice Scattering in Homopolar Semiconductors, *Proc. Phys. Soc. London B* 68, 675-680 (1955).

A-2. Barrie, R., Electronic Conduction in Solids with Spherically Symmetric Band Structure, *Proc. Phys. Soc. London B* 69, 553-561 (1956).

A-3. Replacement of the energy-independent effective mass of the parabolic band by the energy-dependent effective mass of the non-parabolic band is not the only correction which should be made in calculating the relaxation time. The scattering probability must also be modified by using the proper carrier wave functions for a non-parabolic band. [Zawadski, W., and Szymanska, W., *Phys. Status Solidi B* 45, 415 (1971)].

A-4. Lax, B., and Mavroides, J. G., Statistics of Galvanomagnetic Effects in Germanium and Silicon with Warped Energy Surfaces, *Phys. Rev.* 101, 1650-1657 (1955).

A-5. Cardona, M., Paul, W., and Brooks, H., The Temperature Dependence of Polarizability of the Free Carriers in Germanium and Silicon, *Helv. Phys. Acta* 33. 329-346 (1960).

A-6. Hensel, J. C., and Feher, G., Cyclotron Resonance Experiments in Uniaxially Stressed Silicon: Valence Band Inverse Mass Parameters and Deformation Potentials, *Phys. Rev.* 129, 1041-1062 (1963).

A-7. Armstrong, D. B., and Champlin, K. S., *J. Appl. Phys.* 37, 911 (1966).

A-8. Nathan, J. I., Paul, W., and Brooks, H., *Am. Phys. Soc. Bull.* 3, 14 (1958).

A-9. Barber, H. D., Effective Mass and Intrinsic Concentration in Silicon, *Solid State Electronics* 10, 1039-1051 (1967).

A-10. Costato, M., and Reggiani, E., Temperature-Dependence of the Combined Effective Mass of Holes in Silicon, *Lettere al Nuovo Cimento* 3, 239-245 (1970).

A-11. Li, S. S., The Dopant Density and Temperature Dependence of Resistivity and Hole Mobility in Boron-Doped Silicon, *Solid State Electronics* 21, 1109-1118 (1978).

A-12. Kane, E. O., Energy Band Structure in p-Type Germanium and Silicon, *J. Phys. Chem. Solids* 1, 82-99 (1956).

A-13. Dresselhaus, G., Kip, A. F., and Kittel, C., Spin-Orbit Interaction and the Effective Masses of Holes in Germanium, *Phys. Rev.* 95, 568 (1954).

A-14. Balslev, I., and Lewaetz, P., On the Interpretation of the Observed Hole Mass Shift with Uniaxial Stress in Silicon, *Phys. Letters* 19, 6 (1965).

A-15. Wiley, J. D., Mobility of Holes in III-V Compounds, *Semiconductors and Semimetals*, R. K. Willardson and A. C. Beer, Eds., Vol. 10, 91-194 (Academic Press, New York, 1975).

A-16. Cardona, M., and Pollak, F. H., Energy-Band Structure of Germanium and Silicon: The k.p Method, *Phys. Rev.* 142, 530-543 (1966).

A-17. Swerdling, S., Button, K. J., Lax, B., and Roth, L. M., Internal Impurity Levels in Semiconductors: Experiments in p-Type Silicon, *Phys. Rev. Letters* 4, 173 (1960).

A-18. Gagliani, G., and Reggiani, L., Nonparabolicity and Intrinsic Carrier Concentration in Si and Ge, *Nuovo Cimento* 30, 207-216 (1975).

A-19. Miyazawa, H., Suzuki, K., and Maeda, H., Evidence for the <100> Swelling Constant Energy Surface for Heavy Holes in Silicon, *Phys. Rev.* 131, 2442-2444 (1963).

A-20. Balslev, I., Influence of Uniaxial Stress on the Indirect Absorption Edge in Silicon and Germanium, *Phys. Rev.* 143, 636-647 (1966).

A-21. Adler, E., and Erlbach, E., Polarization Dependence of the Indirect Piezoabsorption Coefficient in Ge and Si, *Phys. Rev. Letters* 16, 87 (1966).

A-22. Seeger, K., *Semiconductor Physics* (Springer-Verlag, New York, 1973).

A-23. Bube, R. H., *Electronic Properties of Crystalline Solids* (Academic Press, New York, 1974).

A-24. Long, D., Galvanomagnetic Effects in p-Type Silicon, *Phys. Rev.* 107, 672-677 (1957).

A-25. Hauge, P., Magneto-kerr Effect Study in *P*-Type Silicon, Ph.D., Thesis, The University of Minnesota, Minneapolis, Minnesota (1967).

NBS-114A (REV. 9-78)

U.S. DEPT. OF COMM. BIBLIOGRAPHIC DATA SHEET	1. PUBLICATION OR REPORT NO. SP-400-47	2. Gov't. Accession No.	3. Recipient's Accession No.

4. TITLE AND SUBTITLE

Semiconductor Measurement Technology:
The Theoretical and Experimental Study of the Temperature and Dopant Density Dependence of Hole Mobility, Effective Mass, and Resistivity in Boron-Doped Silicon

5. Publication Date November 1979

6. Performing Organization Code

7. AUTHOR(S)

Sheng S. Li

8. Performing Organ. Report No.

9. PERFORMING ORGANIZATION NAME AND ADDRESS

University of Florida
Electrical Engineering Dept.
Gainesville, FL 32611

10. Project/Task/Work Unit No.

11. Contract/Grant No.
7-35741 - ARPA
ENG76-81828 - NSF

12. SPONSORING ORGANIZATION NAME AND COMPLETE ADDRESS *(Street, City, State, ZIP)*

NBS - Washington, DC 20234
ARPA - Arlington, VA 22209
National Science Foundation - Washington, DC 20550

13. Type of Report & Period Covered
Final

14. Sponsoring Agency Code

15. SUPPLEMENTARY NOTES

This work was funded by the Defense Advanced Research Projects Agency under ARPA Order 2397, Program Code 7Y10.

☐ Document describes a computer program; SF-185, FIPS Software Summary, is attached.

16. ABSTRACT *(A 200-word or less factual summary of most significant information. If document includes a significant bibliography or literature survey, mention it here.)*

Theoretical expressions for computing resistivity and conductivity mobility of holes as functions of dopant density and temperature have been derived for boron-doped silicon. The model is applicable for dopant densities from 10^{13} to 3×10^{18} cm^{-3} and temperatures between 100 and 400 K.

Using a three-band [i.e., heavy-hole, light-hole, and spin-orbit split (SO) bands] model, the hole mobility was calculated by properly combining the contributions from scattering by lattice phonons, ionized impurities, and neutral impurities. In addition, the effects of hole-hole (h-h) scattering and nonparabolicity of the light-hole band were taken into account in the mobility formulation.

To verify our theoretical calculations, resistivity measurements on nine boron-doped silicon slices with dopant densities from 4.5×10^{14} to 3.2×10^{18} cm^{-3} were performed for $100 \leq T \leq 400$ K, using a planar four-probe square-array test structure. Agreement between our calculated and measured resistivity values was within 6 percent over the entire range of dopant density and temperature studied here. Excellent agreement (within ±5 percent) between our calculated hole mobility values and those of Thurber *et al.* was obtained for $N_A \leq 10^{18}$ cm^{-3}. These discrepancies are attributed to Wagner's neglect of the effect of deionization of boron impurities at

(over)

17. KEY WORDS *(six to twelve entries; alphabetical order; capitalize only the first letter of the first key word unless a proper name; separated by semicolons)*

Boron-doped silicon; dopant density; effective mass; hole mobility; ionized impurity scattering mobility; lattice scattering mobility; neutral impurity scattering mobility; *p*-type silicon; resistivity; scattering mechanisms.

18. AVAILABILITY

☒ Unlimited

☐ For Official Distribution. Do Not Release to NTIS

☒ Order From Sup. of Doc., U.S. Government Printing Office, Washington, DC 20402, SD Stock No. SN003-003-02140-7

☐ Order From National Technical Information Service (NTIS), Springfield, VA. 22161

19. SECURITY CLASS (THIS REPORT)	21. NO. OF PRINTED PAGES
UNCLASSIFIED	50
20. SECURITY CLASS (THIS PAGE)	**22. Price**
UNCLASSIFIED	$2.25

USCOMM-DC

U.S. DEPT. OF COMM.
BIBLIOGRAPHIC DATA SHEET

16. ABSTRACT (continued)

higher dopant densities (i.e., he assumed hole density equal to the total boron density).

Finally, formulations for the density-of-states effective mass, conductivity effective mass, and Hall effective mass are described, and the results are applied to the calculations of hole masses in boron-doped silicon for $10^{14} \leq N_A \leq 10^{18}$ cm^{-3} and $50 \leq T \leq 500$ K.

Announcement of Semiconductor Measurement Technology
List of Publications 72 – 1962-1979

Chief
Electron Devices Division
National Bureau of Standards
Bldg. 225, Room A305
Washington, DC 20234

Dear Sir:

Please send a copy of your latest "Semiconductor Measurement Technology, List of Publications 72."

Name _____

Company _____

Address _____

City _____ State _____ Zip Code _____

NBS TECHNICAL PUBLICATIONS

PERIODICALS

JOURNAL OF RESEARCH—The Journal of Research of the National Bureau of Standards reports NBS research and development in those disciplines of the physical and engineering sciences in which the Bureau is active. These include physics, chemistry, engineering, mathematics, and computer sciences. Papers cover a broad range of subjects, with major emphasis on measurement methodology and the basic technology underlying standardization. Also included from time to time are survey articles on topics closely related to the Bureau's technical and scientific programs. As a special service to subscribers each issue contains complete citations to all recent Bureau publications in both NBS and non-NBS media. Issued six times a year. Annual subscription: domestic $17; foreign $21.25. Single copy, $3 domestic; $3.75 foreign.

NOTE: The Journal was formerly published in two sections: Section A "Physics and Chemistry" and Section B "Mathematical Sciences."

DIMENSIONS/NBS—This monthly magazine is published to inform scientists, engineers, business and industry leaders, teachers, students, and consumers of the latest advances in science and technology, with primary emphasis on work at NBS. The magazine highlights and reviews such issues as energy research, fire protection, building technology, metric conversion, pollution abatement, health and safety, and consumer product performance. In addition, it reports the results of Bureau programs in measurement standards and techniques, properties of matter and materials, engineering standards and services, instrumentation, and automatic data processing. Annual subscription: domestic $11; foreign $13.75.

NONPERIODICALS

Monographs—Major contributions to the technical literature on various subjects related to the Bureau's scientific and technical activities.

Handbooks—Recommended codes of engineering and industrial practice (including safety codes) developed in cooperation with interested industries, professional organizations, and regulatory bodies.

Special Publications—Include proceedings of conferences sponsored by NBS, NBS annual reports, and other special publications appropriate to this grouping such as wall charts, pocket cards, and bibliographies.

Applied Mathematics Series—Mathematical tables, manuals, and studies of special interest to physicists, engineers, chemists, biologists, mathematicians, computer programmers, and others engaged in scientific and technical work.

National Standard Reference Data Series—Provides quantitative data on the physical and chemical properties of materials, compiled from the world's literature and critically evaluated. Developed under a worldwide program coordinated by NBS under the authority of the National Standard Data Act (Public Law 90-396).

NOTE: The principal publication outlet for the foregoing data is the Journal of Physical and Chemical Reference Data (JPCRD) published quarterly for NBS by the American Chemical Society (ACS) and the American Institute of Physics (AIP). Subscriptions, reprints, and supplements available from ACS, 1155 Sixteenth St., NW, Washington, DC 20056.

Building Science Series—Disseminates technical information developed at the Bureau on building materials, components, systems, and whole structures. The series presents research results, test methods, and performance criteria related to the structural and environmental functions and the durability and safety characteristics of building elements and systems.

Technical Notes—Studies or reports which are complete in themselves but restrictive in their treatment of a subject. Analogous to monographs but not so comprehensive in scope or definitive in treatment of the subject area. Often serve as a vehicle for final reports of work performed at NBS under the sponsorship of other government agencies.

Voluntary Product Standards—Developed under procedures published by the Department of Commerce in Part 10, Title 15, of the Code of Federal Regulations. The standards establish nationally recognized requirements for products, and provide all concerned interests with a basis for common understanding of the characteristics of the products. NBS administers this program as a supplement to the activities of the private sector standardizing organizations.

Consumer Information Series—Practical information, based on NBS research and experience, covering areas of interest to the consumer. Easily understandable language and illustrations provide useful background knowledge for shopping in today's technological marketplace.

Order the **above** *NBS publications from: Superintendent of Documents, Government Printing Office, Washington, DC 20402.*

Order the **following** *NBS publications—FIPS and NBSIR's—from the National Technical Information Services, Springfield, VA 22161.*

Federal Information Processing Standards Publications (FIPS PUB)—Publications in this series collectively constitute the Federal Information Processing Standards Register. The Register serves as the official source of information in the Federal Government regarding standards issued by NBS pursuant to the Federal Property and Administrative Services Act of 1949 as amended, Public Law 89-306 (79 Stat. 1127), and as implemented by Executive Order 11717 (38 FR 12315, dated May 11, 1973) and Part 6 of Title 15 CFR (Code of Federal Regulations).

NBS Interagency Reports (NBSIR)—A special series of interim or final reports on work performed by NBS for outside sponsors (both government and non-government). In general, initial distribution is handled by the sponsor; public distribution is by the National Technical Information Services, Springfield, VA 22161, in paper copy or microfiche form.

BIBLIOGRAPHIC SUBSCRIPTION SERVICES

The following current-awareness and literature-survey bibliographies are issued periodically by the Bureau:

Cryogenic Data Center Current Awareness Service. A literature survey issued biweekly. Annual subscription: domestic $25; foreign $30.

Liquefied Natural Gas. A literature survey issued quarterly. Annual subscription: $20.

Superconducting Devices and Materials. A literature survey issued quarterly. Annual subscription: $30. Please send subscription orders and remittances for the preceding bibliographic services to the National Bureau of Standards, Cryogenic Data Center (736) Boulder, CO 80303.

U.S. DEPARTMENT OF COMMERCE
National Bureau of Standards
Washington, D.C. 20234

OFFICIAL BUSINESS

Penalty for Private Use, $300

POSTAGE AND FEES PAID
U.S. DEPARTMENT OF COMMERCE
COM-215

U.S.MAIL

SPECIAL FOURTH-CLASS RATE
BOOK